Classification of aerosol radiative properties during African desert dust intrusions over southeastern Spain by sector origins and cluster analysis

A. Valenzuela,[1,2] F. J. Olmo,[1,2] H. Lyamani,[1,2] M. Antón,[1,2] A. Quirantes,[1] and L. Alados-Arboledas[1,2]

Received 17 September 2011; revised 27 December 2011; accepted 30 January 2012; published 28 March 2012.

[1] The main goal of this study is to analyze the dependence of columnar aerosol optical and microphysical properties on source region and transport pathways during desert dust intrusions over Granada (Spain) from January 2005 to December 2010. Columnar aerosol properties have been derived from a non-spherical inversion code using the solar extinction measurements and sky radiances in the principal plane. Two classification methods of the African air masses ending at the study location were used by means of the HYSPLIT back-trajectories analysis. The first one, based on desert dust origin sources, discriminated the optical properties only for sector B (corresponding to western Sahara, northwest Mauritania and southwest Algeria). The particles present marked absorbing properties (low value of single scattering albedo at all wavelengths) during the desert dust events when the air masses were transported from sector A (north Morocco, northwest Algeria). This result may be related to the mixing of desert dust with anthropogenic pollutants from North African industrial areas in addition to the mixing with local anthropogenic aerosol and pollutants transported from European and Mediterranean areas. The second classification method was based on a statistics technique called cluster classification which allows grouping the air masses back trajectories with similar speed and direction of the trajectory. This method showed slight differences in the optical properties between the several transport pathways of air masses. High values of the aerosol optical depth and low mean values of the Angström parameter were associated with longer transport pathways over desert dust sources and slowly moving air masses. Both classification methods showed that the fine mode was mixed with coarse mode, being the fine mode fraction smaller than 55%.

Citation: Valenzuela, A., F. J. Olmo, H. Lyamani, M. Antón, A. Quirantes, and L. Alados-Arboledas (2012), Classification of aerosol radiative properties during African desert dust intrusions over southeastern Spain by sector origins and cluster analysis, *J. Geophys. Res.*, *117*, D06214, doi:10.1029/2011JD016885.

1. Introduction

[2] Desert dust is one the major aerosol components in the global atmosphere that affects the Earth's climate through interacting with both solar and thermal infrared radiation. The North Africa dust is the most important source of mineral dust in the Northern Hemisphere [e.g., *Liu et al.*, 2008]. The continuous measurements recorded during the SAMUM campaign (May/June 2006, Morocco) provided an excellent opportunity to analyze the height that can reach the dust particles when they are injected to the atmosphere from the potential sources of emission [*Knippertz et al.*, 2009; *Tesche et al.*, 2009]. The results of the campaign revealed that the depth of the dust layer usually reaches a height of 4–6 km above sea level, even sometimes up to 7 km. Dust is then transported in a wide range of different altitudes (up to 5 km) to other areas [*Escudero et al.*, 2005, 2011]. The Iberian Peninsula is frequently affected by North African dust episodes with large aerosol load that can modulate the aerosol climatology in different areas, especially in southern Spain [*Lyamani et al.*, 2005; *Toledano et al.*, 2007a; *Cachorro et al.*, 2008] and Portugal [*Wagner et al.*, 2009]. Lidar observations have been utilized to characterize the vertical layering structure during desert dust events over Granada [*Guerrero-Rascado et al.*, 2009; *Córdoba-Jabonero et al.*, 2011]. These authors have shown that the dust layers are confined between 2.5 and 4.5 km heights and peaking about at 3.2 km. On a global average, mineral dust is responsible for approximately one third of global extinction optical depth [*Tegen et al.*, 1997] in the mid-visible wavelengths,

[1]Departamento de Física Aplicada, Universidad de Granada, Granada, Spain.
[2]Also at Centro Andaluz de Medio Ambiente, Granada, Spain.

0148-0227/12/2011JD016885

and absorbs significantly in the blue and ultraviolet wavelengths due to iron oxide impurities [*Sokolik and Toon*, 1999]. Close to the source region mostly pure dust is found, but after a long range transport the aging of the dust and mixing with other aerosol types modify the optical properties of the desert dust [*Bauer et al.*, 2011; *Hand et al.*, 2010]. The mixing of desert dust with anthropogenic particles may prompt changes in the physical properties and chemical composition of the desert dust and this may have important consequences in processes affecting climate [*Rodriguez et al.*, 2011; *Gu et al.*, 2010]. Knowledge of the optical and microphysical properties of these aerosol mixtures is particularly important for assessing their direct and indirect radiative forcing. Mixtures of desert dust and combustion aerosols contain the two primary particulate absorbing species: black carbon in fine mode particles [*Bond and Bergstrom*, 2006] and iron oxides in coarse mode particles [*Sokolik and Toon*, 1999]. Analysis of mineral dust and biomass burning particles mixings with respect to their impact on radiative forcing was performed at Granada, Spain by *Lyamani et al.* [2006].

[3] The analysis of air mass back-trajectories is a powerful tool commonly used to study the atmospheric aerosol and aerosol transport from an origin source to receptor sites. Previous studies [e.g., *Estellés et al.*, 2007; *Toledano et al.*, 2009] identified the air mass origin sector by considering the time spent over the source. Other works have taken into account the altitude of the air masses and the possible interactions with the boundary layer [*Pace et al.*, 2006]. Although the dust injection height can reach up to 7 km in the sources, the authors used as reference minimum height (1000 m a.s.l.) of air masses trajectories which interact with the mixed layer [*Petzold et al.*, 2009]. Other relevant method of the air masses classification is the cluster analysis [e.g., *Dorling et al.*, 1992; *Mattis et al.*, 2000; *Rozwadowska et al.*, 2010; *Bösenberg et al.*, 2003]. Using this methodology, *Toledano et al.* [2009] established as representative of Saharan air masses trajectories the 1500 and 3000 m levels.

[4] Laboratory measurements revealed that the shapes of dust particles are irregular [*Koren et al.*, 2001; *Muñoz et al.*, 2001]. During SAMUM campaign, *Kandler et al.* [2009] showed elongated shapes for dust particles using measurements of the particle aspect ratio, which can be attributed to their chemical composition and origin. A detailed theoretical study on the optical properties of dust particles based on a spheroid polydispersion model has shown that the scattering properties of non-spherical dust particles are significantly different to those obtained by Lorenz-Mie model considering dust as spheres [*Mishchenko et al.*, 1997]. *Silva et al.* [2002] established that the nonsphericity of aerosol particles gives an additional contribution to the negative shortwave radiative forcing. Neglecting the non-sphericity of desert dust may result in a substantial underestimation or overestimation of dust radiative forcing [*von Hoyningen-Huene and Posse*, 1997, 1999].

[5] Numerous works have derived radiative properties of desert dust from measurements of sky radiance in the almucantar configuration [e.g., *von Hoyningen-Huene and Posse*, 1997, 1999; *Silva et al.*, 2002; *Dubovik et al.*, 2002a; *Kubilay et al.*, 2003; *Lyamani et al.*, 2005; *Tafuro et al.*, 2006; *Olmo et al.*, 2006; *Toledano et al.*, 2007a, 2007b; *Cachorro et al.*, 2008; *Pinker et al.*, 2010; *Eck et al.*, 2010; *Garcia et al.*, 2011]. However, only a few authors have used the sky radiance in the principal plane configuration [*Olmo et al.*, 2008; *Valenzuela et al.*, 2011, 2012]. *Olmo et al.* [2006, 2008] analyzed the columnar aerosol radiative properties at Granada using sky radiance in both almucantar and principal plane configurations. These authors reported that the aerosol properties obtained using the two configurations showed a good agreement. The main application of the sky radiance measurements in the principal plane configuration is the retrieval of atmospheric aerosol radiative properties along the day, not just for large solar zenith angles and the validation of the aerosol information retrieved from satellite sensors (e.g., MISR and POLDER) due to the relatively small solar zenith angles corresponding to their overpass time [*Sinyuk et al.*, 2007]. Therefore, inversion techniques using the principal plane configuration will play an outstanding role in the near future.

[6] The main objective of this work is to analyze the columnar aerosol optical and microphysical properties during desert dust intrusions in southeastern Spain taking into account the origin sources and the transport pathways of the African air mass affecting our study area and the associated synoptic conditions that favored the arrival of these African air masses. The period of study is 2005–2010. Columnar radiative properties have been computed using the extinction measurements and sky radiance in the principal plane configuration by means of a non-spherical inversion code [*Olmo et al.*, 2006, 2008]. Air mass back-trajectories ending at Granada were calculated using the hybrid single particle Lagrangian integrated trajectory model (HYSPLIT_4) when aerosol optical data were available [*Draxler and Hess*, 1998]. Two classification methods were used. The first is based on the identification of dust origin sources [*Pace et al.*, 2006] and the second is based on cluster analysis. Therefore, this work will contribute to improve the understanding about the possible dependence on the aerosol optical and microphysical properties during desert dust events according to the dust source regions and air masses pathways. The paper has the following structure: the experimental site and instrumentation are described in section 2, and methodology in section 3. The results and discussion are given in section 4, with concluding remarks made in section 5.

2. Experimental Site and Instrumentation

[7] Solar extinction and sky radiance measurements have been performed in the urban area of Granada (37.18°N, 3.58°W and 680 m a.s.l.). Granada, located in southeastern Spain, is a non-industrialized and medium-sized city with 250000 inhabitants (twice including its metropolitan area). The city is situated in a natural basin surrounded by mountains with altitudes over 1000 m. The near-continental conditions prevailing at this site are responsible for large seasonal temperature differences, providing cool winters and hot summers. The study area is about 200 km away from the African continent, and approximately 50 km away from the western Mediterranean basin. Due to its proximity to the Iberian Peninsula, the North African constitutes a potential source of mineral particles under certain meteorological scenarios [*Rodriguez et al.*, 2001; *Escudero et al.*, 2005]. southern Spain is more frequently affected by air masses

from North Africa than other regions of the Iberian Peninsula [*Querol et al.*, 2004]. The following meteorological scenarios favor the North African desert dust transport over the Iberian Peninsula; a North African high pressure located at surface levels, an Atlantic depression located in front Portugal, a North African depression, and a North African high pressure situated at upper levels [*Escudero et al.*, 2005].

[8] Column-integrated characterization of the atmospheric aerosol has been performed by means of a Sun photometer CIMEL CE-318-4 included in the AERONET network [*Holben et al.*, 1998]. This Sun photometer makes direct sun measurements every 15 min with a 1.2° full field of view at 340, 380, 440, 670, 870, 940 and 1020 nm. The full-width at half-maximum of the interference filters are 2 nm at 340 nm, 4 nm at 380 nm and 10 nm at all other wavelengths. In addition, the CIMEL instrument performs sky radiances, both in almucantar and principal plane, at 440, 670, 870 and 1020 nm following an optical air mass protocol showed by *Holben et al.* [1998]. Calibration of this instrument was performed by AERONET. More details about CIMEL CE-318-4 are given by *Holben et al.* [1998].

3. Methodology

[9] In this paper we focus on African dust events from January 2005 to December 2010 that have been confirmed by CALIMA network (www.calima.ws) on southeastern of the Spain. The CALIMA network produces periodically reports on the 24 h forecasts of dust outbreaks (e-mail alerts sent to air quality networks 24 h in advance). Later, the CALIMA network produces a report of validations taking into account the different Spanish areas. To perform these reports the network uses the information on the PM10 levels recorded at regional background stations in Spain, the HYSPLIT4 model [*Draxler and Rolph*, 2003] (http://www.arl.noaa.gov/ready/hysplit4.html), synoptic meteorological charts (http://www.ecmwf.int/), the maps of aerosol index of Ozone Monitoring Instrument (OMI) (ftp://toms.gsfc.nasa.gov/pub/omi/images/aerosol/), the SeaWiFS maps information (http://oceancolor.gsfc.nasa.gov/SeaWiFS/HTML/dust.htlm), the daily results of the aerosol models outputs such as SKIRON (http://forecast.uoa.gr), BSC-DREAM (http:// www.bsc.es/projects/earthscience/DREAM/) and NAAPs (http:// www.nrlmry.navy.mil/aerosol/), and, finally, the levels of PM10 recorded at regional background stations from air quality monitoring. Therefore, the reports of validated days correspond to African desert dust events tested by models, back-trajectories analysis, synoptic meteorological charts, satellite and surface data.

[10] From the Sun photometer solar extinction measurements, the aerosol optical depth (AOD) at selected spectral channels and the Angström parameter (α) have been computed following the method described by *Alados-Arboledas et al.* [2003, 2008] and *Estellés et al.* [2006]. All measurements sequences are carried out following the AERONET protocols. The Sun photometer was calibrated by the AERONET team, and a linear rate change was assumed for the calibration coefficients. Pre- and post-field calibration, automatically cloud cleared and manually inspected were applied (similar procedure to AERONET level 2.0 AOD data).

[11] The most relevant error in the calculation of the aerosol optical properties comes from the calibration uncertainties. The AOD (λ) absolute errors can be derived from Beer-Bouguer-Lambert law by error propagation theory [*Reagan et al.*, 1986; *Duran*, 1997]. These results show that the uncertainty values for each wavelength are different, depending on the processes involved. In our case, the combined effects result in a total uncertainty in AOD of about ± 0.01 for $\lambda > 440$ nm and ± 0.02 for shorter wavelengths, similar to AERONET level 2.0 data [*Holben et al.*, 1998].

[12] The retrieval of the columnar aerosol radiative properties from sky radiances requires accurate correction for the effects of multiple scattering and for the contribution of light reflected from the Earth's surface and scattered downward in the atmosphere. *Nakajima et al.* [1996] developed an inversion scheme for spherical particles that includes accurate radiative transfer modeling in order to account for multiple scattering effects. *Olmo et al.* [2006, 2008] adapted this method to take into account non-spherical particles. This inversion procedure uses the spectral AOD and the normalized spectral spectral sky radiances in almucantar and principal planes.

[13] For the inversion retrieval the method uses the relative diffuse sky radiance (normalized by direct irradiance), $R(\Theta)$, that is less affected by deterioration of the interference filters of the Sun photometer, i.e.,

$$R(\Theta) = \beta(\Theta) + q(\Theta), \tag{1}$$

where is the total differential scattering coefficient, that is the sum of the scattering coefficients for aerosol and for molecules. The aerosol optical thickness, AOD (λ) is defined as

$$AOD(\lambda) = \frac{2\pi}{\lambda} \int_{r_{\min}}^{r_{\max}} k_{ext}(x,m)v(r)d\ln r, \tag{2}$$

where x is the size parameter, v(r)(=dV/d lnr (cm3 cm−2)) is the columnar volume spectrum (aerosol size distribution), m is the complex refractive index, K(x, m) is the kernel function, and r_{min} and r_{max} are minimum and maximum aerosol radii. The kernel function K_{ext} is defined as

$$K_{ext}(x,m) = \frac{3}{4}\frac{Q_{ext}(x)}{x}, \tag{3}$$

where Q_{ext} is the extinction efficiency. Also, in this method, the aerosol differential scattering coefficient is expressed

$$\beta_A(\Theta) = \frac{2\pi}{\lambda} \int_{r_{\min}}^{r_{\max}} k_{ext}(\Theta,x,m)v(r)d\ln r, \tag{4}$$

where K is the kernel function.

[14] The algorithm retrieves the columnar size volume distributions from aerosol differential scattering coefficient, and AOD (λ) using an iterative inversion scheme. As the extinction coefficient can be expressed as the sum of scattering and absorption coefficients, aerosol optical thickness for the scattering can be obtained using equation (2) with the kernel function of scattering, and thus

we can derive the monochromatic single scattering albedo [*Kim et al.*, 2004].

[15] EBCM, or T-matrix, has been used to calculate light scattering for non-spherical matrices (kernel matrices) instead of Mie simulations by Nakajima [*Nakajima et al.*, 1996; *Kim et al.*, 2004]. Accordingly, the aerosol single-scattering properties are defined as functions of the volume size distribution of randomly oriented polydisperse spheroids. Following the recommendations of *Dubovik et al.* [2002b], the kernel matrices are computed for randomly oriented prolate and oblate spheroids with aspect ratios ranging from 0.6 to 1.66, using equiprobable distributions.

[16] For the complex refractive index the selected value is invariant with wavelength. The optimal value is retrieved by iteration, minimizing the residuals between measured and simulated normalized radiances. The equation of the residuals is

$$\Delta = \sqrt{\frac{\sum_{\lambda,\Theta}[(R_{\lambda\Theta} - C_{\lambda\Theta})/R_{\lambda\Theta}]}{N_\lambda N_\Theta}} \quad (5)$$

where R is the measured and C the calculated normalized experimental sky radiance, and N is the number of wavelengths and scattering angles measured. The refractive indices used in the iterative process are: 1.33–1.55 (0.02 step) and 0–0.01 (0.0005 step) for the real part and imaginary part, respectively. The algorithm retrieves first the real part of the refractive index -assuming the imaginary part as zero- and then, fixing the real part, the imaginary part is retrieved.

[17] A large set of columnar aerosol radiative parameters during the African dust intrusions were derived from the non-spherical inversion code proposed by *Olmo et al.* [2008] and sky radiance measurements in principal plane configuration. The retrieved columnar aerosol microphysical and optical properties include volume size distribution, single scattering albedo, $\omega_0(\lambda)$, and asymmetry parameter, $g(\lambda)$. Single scattering albedo is one of the fundamental parameter to quantify aerosol light absorption. The mineral dust interacts with solar and terrestrial radiation field. Mineral particles can be strong and weak light absorbers depending of their mineralogical composition and the spectral range. This situation will determine the sign of radiative forcing. Therefore, mineral dust can lead to either cooling or warming of the Earth's atmosphere [*Müller et al.*, 2009]. From the retrieved volume aerosol size distributions, the effective radius and the modal radius as well as the volume concentration for total, fine and coarse modes were derived following the procedure of *Dubovik et al.* [2002b]. The cutoff radius used in size distributions for fine and coarse modes was 0.5 μm.

[18] Moreover, we have used a graphical framework presented for [*Gobbi et al.*, 2007] to obtaining additional aerosol properties using AOD information. The classification scheme is sensitive to refractive index. This have been computed for refractive index $m = 1.4 - 0.001i$. In addition, these calculations are made assuming spherical particles. The degree of indetermination of this classification scheme is of the order of 25% for r_f (fine modal radius) and 10% for η (fine mode fraction) with refractive index varying between $m = 1.33 - 0.0i$ and $m = 1.53 - 0.003i$. Their method uses a combined analysis of α and its spectral curvature represented by $\delta\alpha$. This allows to infer aerosol fine mode size and their fractional contribution to the total AOD. In addition, their method separate increases due to fine-mode humidification from AOD increases due to the increase in coarse particles. It should be noted that for AOD < 0.10, the errors associated to α and $\delta\alpha$ are ~20% and 50%, respectively.

[19] Five-day back-trajectories of air masses arriving at Granada at 500, 1500 and 3000 m a.g.l. were calculated using HYSPLIT_4 model including vertical wind [*Draxler and Hess*, 1998] coincident with African desert dust days established by CALIMA network. The NCEP/NCAR reanalysis database was used as model input (NOAA Operational Model Archive Distribution System server at NCEP). For each day, one single trajectory at each height level was computed with endpoint in Granada at 12:00 UTC. Most aerosol content is within boundary layer, however, desert dust aerosol can be transported a higher altitudes [*Escudero et al.*, 2011]. For this reason, we computed trajectories at 500, 1500, and 3000 m a.g.l., corresponding to pressure levels at approximately 950, 850 and 700 hPa, respectively. Numerous authors have computed trajectories between 500 and 3000 m a.g.l. for African air masses arriving at Iberian Peninsula [*Escudero et al.*, 2011; *Toledano et al.*, 2009; *Guerrero-Rascado et al.*, 2009; *Wagner et al.*, 2009]. After, we have performed a visual inspection of the air masses trajectories at all levels. We have checked that the 500 m a.g.l. air masses arriving at Granada never over pass for the North Africa. Therefore, we have only classified African air masses at 1500 and 3000 m a.g.l. arriving at Granada. Finally, to verify that input of dust, we have exploited MODIS satellite imagery products and we have compared them with air masses trajectories transported from North Africa.

[20] We have classified the columnar aerosol radiative properties using two different methodologies: (1) taking into account the dust source region, and (2) the air mass transport pathway.

3.1. Identification of Desert Dust Origin Sources

[21] We used the criteria of *Pace et al.* [2006] to identify desert dust source sectors. This method assume that the dust particles are confined in the mixed layer at the source region, and that the air mass is loaded by desert dust when the air mass altitude, $z_{back\text{-}traj}$, is lower or close to the altitude of the mixed layer, z_{mxl}, (entrainment condition). The geographical sector where the entrainment condition is met along the trajectory is identified as the source of the observed aerosol. If the entrainment condition is met at more than one point, the geographical position where the difference ($z_{back\text{-}traj.} - z_{mxl}$) is the lowest (sign included) is selected as the potential source of aerosol particles. In this study, both the air mass back-trajectories and mixed layer altitudes were supplied by the HYSPLIT model. The time spent in 1.5° latitude and longitude square around Granada is excluded from the calculations. We have defined three broad geographical sectors, displayed in Figure 1, in relation to different desert dust sources [*Prospero et al.*, 2002]. The defined sectors are (1) sector A (north Morocco, northwest Algeria), (2) sector B (western Sahara, northwest Mauritania and southwest Algeria) and (3) sector C (eastern Algeria, Tunisia).

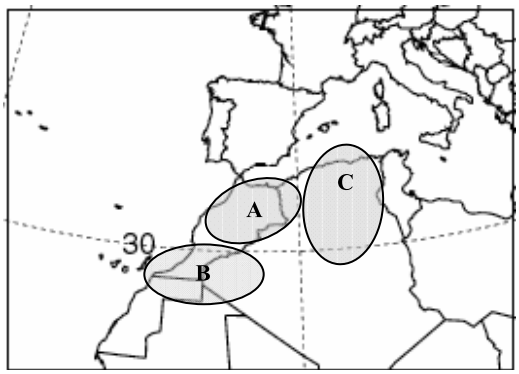

Figure 1. Desert dust origin sources.

3.2. Cluster Analysis

[22] In order to obtain information about airflow patterns on our site, we have applied statistical techniques to a database of individual trajectories from North Africa air masses. This method is based on the geometric distance between individual trajectories and it takes into account speed and direction of the trajectory. The final results are centroids (clusters-mean trajectories) which grouping individual trajectories with similar behavior of their direction and speed of passage over certain areas. The African air masses affecting Granada from 2005 to 2010 were classified according to their transport pathways using HYSPLIT clustering algorithm (http://www.arl.noaa.gov/). The trajectory types are interpretable in terms of the synoptic conditions that form them. Large scale circulation features are associated with certain trajectory clusters. The cluster analysis does not assume the existence of desert dust sources and their geographic locations for clustering the air mass types. However, according this method the researcher chooses the number of cluster that physically represents airflow patterns for the specific site. The centroid represents the average of the trajectories included in that cluster. The HYSPLIT model has a clustering tool based on the variations in both the total variance between clusters (TSV, Spatial Variance Total) and the variance between each component trajectory (SPVAR, Spatial Variance) [*Draxler et al.*, 2009]. First, we have generated a set of 183 back-trajectories arriving over Granada. The grouping process started with an initial number of individual trajectories and ended with the creation of a single cluster that group some of them. In each stage were unified two trajectories that caused the minimum increase of TSV and SPAVR. The appropriate number of clusters here was calculated from the percent change in total spatial variance (TSV) as the sum of the SPVAR. This parameter is derived from the sum of the squared distances between the endpoints of the cluster's component trajectories and the mean of the trajectories in that cluster. Large changes were interpreted as the merging of significantly different trajectories into the same cluster. Accordingly, the approximate number of clusters would be found just prior to the large percent change in TSV. Although the determination of the number of cluster group may be subjective, two groups for each level were chosen in order to a better explanation of the transport regimes during the study period after additional analysis for different cluster numbers. Within each cluster, individual trajectories were averaged to produce a cluster-mean trajectory.

4. Results and Discussion

4.1. Aerosol Properties Classification by Sector Origins

[23] Figure 2 shows the monthly frequencies of African air masses classified by sector origins for the 2005–2010 period. To derive the frequency distributions we have considered only days with desert dust intrusions in which aerosol radiative properties were available. In annual basis, the most frequent African air masses affecting our study area were associated with sector A and B, with an average of occurrence of 47% and 31% for all episodes, respectively. The most frequent synoptic situation in spring and early summer associated with the dust transport to the southeastern of the Iberian Peninsula (from sector A) is a low pressure (observed from sea level to 700 hPa centered southwest of the Portugal coast with an associated high over the central Mediterranean sea). On the other hand, the dust transport from sector B is favored in most cases by an anticyclone (observed from sea level to 700 hPa) centered over North Africa, southeastern Iberian Peninsula and western Mediterranean sea. The most frequent meteorological scenario (22% of all) related to the air masses transport from sector C is a low pressure centered over Morroco and a high (observed from sea level to 850 hPa) centered over eastern of the Algeria and Tunisia (Figure 3). In this last sector the frequency of desert dust events was the lowest throughout the annual cycle. The largest frequency of dust episodes was obtained in July for all sectors, followed by August.

[24] Statistical summary of AOD (440 nm) and α (440–1020 nm), classified by sector origins, are reported in Table 1. In addition, the histograms of relative frequency of these two variables are shown in Figure 4. For all sectors we have found relatively high mean values of AOD (440 nm) and low mean values of α during African dust intrusions. Although the differences obtained in the values AOD (440 nm) and α between the different sectors were within standard deviation, a slightly higher mean AOD

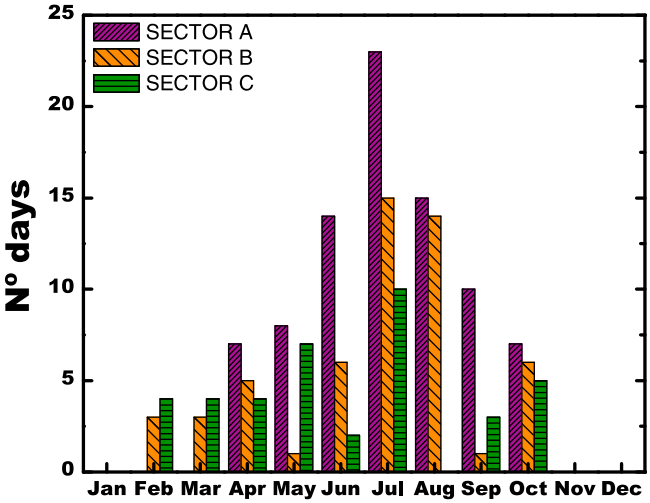

Figure 2. Monthly frequency of African air masses according to the classification by origin sectors.

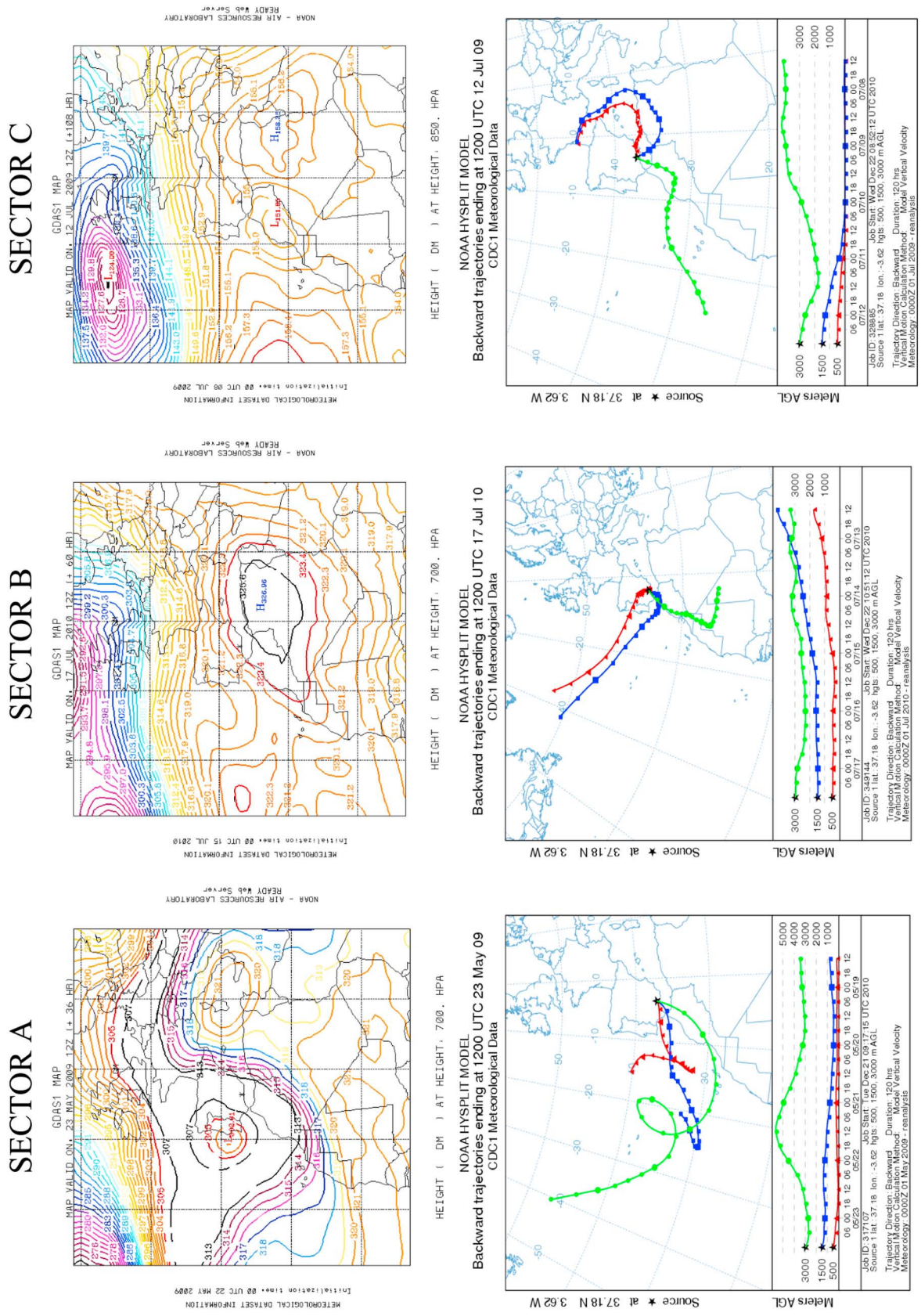

Figure 3. The main synoptic sceneries and back-trajectories at the 500, 1500, and 3000 m levels according to the classification by origin sectors.

Table 1. Statistical Summary of AOD (440 nm) and α (440–1020 nm), Classified by Origin Sectors and Cluster Analysis From 2005 to 2010

							1500 m				3000 m			
	Sector A		Sector B		Sector C		Cluster 1		Cluster 2		Cluster 1		Cluster 2	
	AOD	α	AOD	α	AOD	α	AOD	α	AOD	α	AOD	α	AOD	α
Number of days	86	86	56	56	41	41	56	56	67	67	25	25	35	35
Number of observations	4129	4129	2836	2836	1715	1715	2658	2658	3056	3056	1360	1360	1606	1606
Mean	0.26	0.45	0.29	0.36	0.26	0.46	0.29	0.39	0.24	0.44	0.29	0.38	0.26	0.45
Standard deviation	0.17	0.20	0.13	0.19	0.11	0.23	0.14	0.20	0.16	0.21	0.13	0.20	0.16	0.19
Minimum[a]	0.04	−0.05	0.04	−0.05	0.11	0.03	0.07	−0.08	0.04	−0.05	0.08	0.10	0.05	−0.04
Maximum[b]	1.60	1.04	1.41	1.01	0.98	1.05	2.01	1.05	1.60	1.03	0.79	1.04	1.41	1.03
Median	0.22	0.42	0.28	0.33	0.23	0.43	0.26	0.36	0.20	0.42	0.27	0.33	0.23	0.42

[a]Minimum of the observations.
[b]Maximum of the observations.

(440nm) value of (0.29 ± 0.13) and a slightly lower mean α (440–1020) value of (0.36 ± 0.19) were obtained when air masses were transported from sector B. The Saharan desert (sector B) is the largest source of mineral desert dust [*Goudie and Middleton*, 2001]. It is well known that the dust production and transport in sector B (Saharan desert) experience a marked seasonal evolution. The sources of soil desert dust included into this sector (northern subtropical Saharan latitudes) are activated in summer [*Engelstaedter et al.*, 2006; *Sunnu et al.*, 2008]. The intense heating of the Sahara desert and the consequent development of the North African thermal low and the vertical growth of the boundary layer [*Escudero et al.*, 2005] together high pressure over eastern Algeria and Tunisia favored the air masses transport

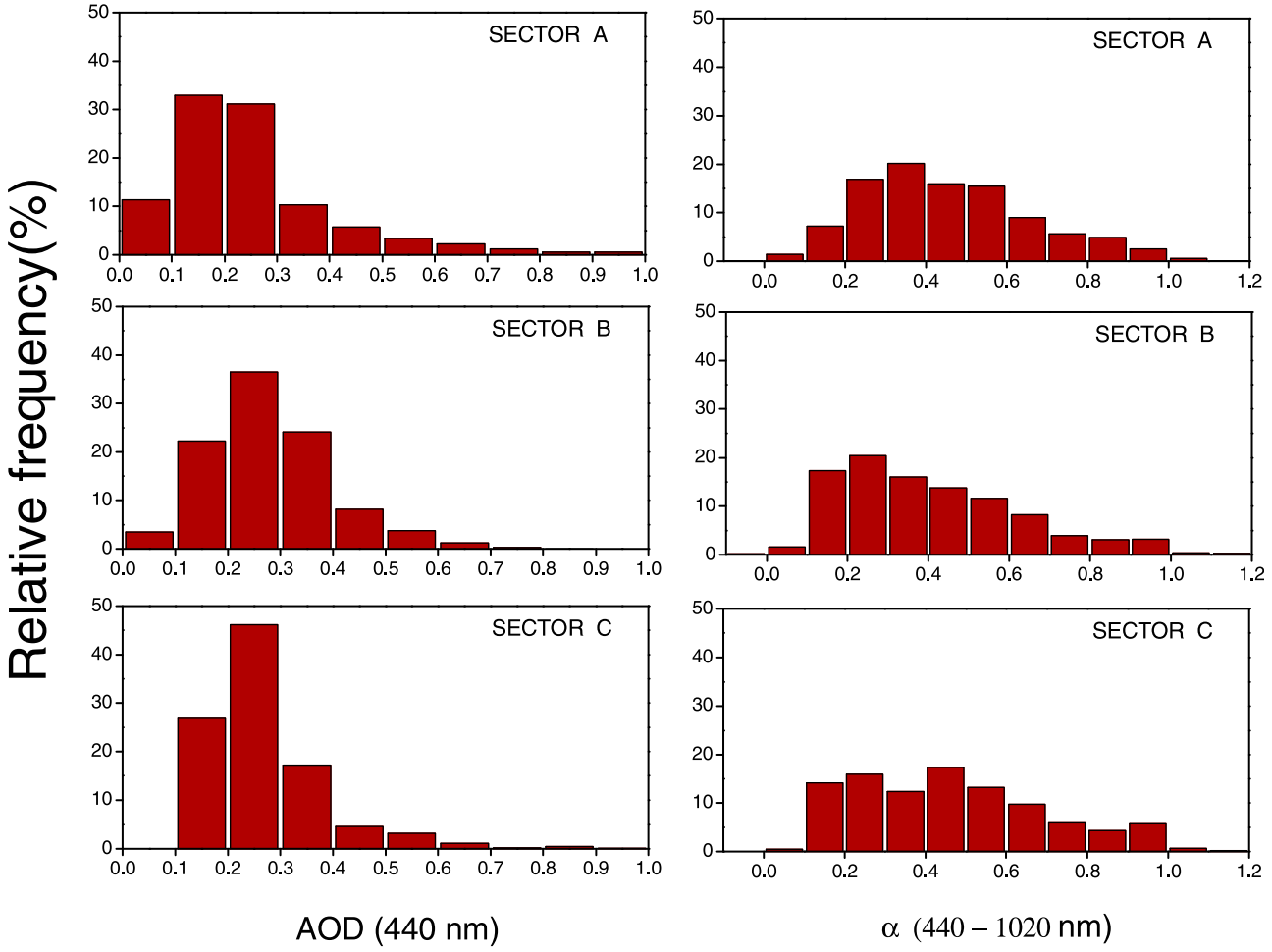

Figure 4. Frequency distribution of AOD (440 nm) and α (440–1020 nm) according to the classification by origin sectors.

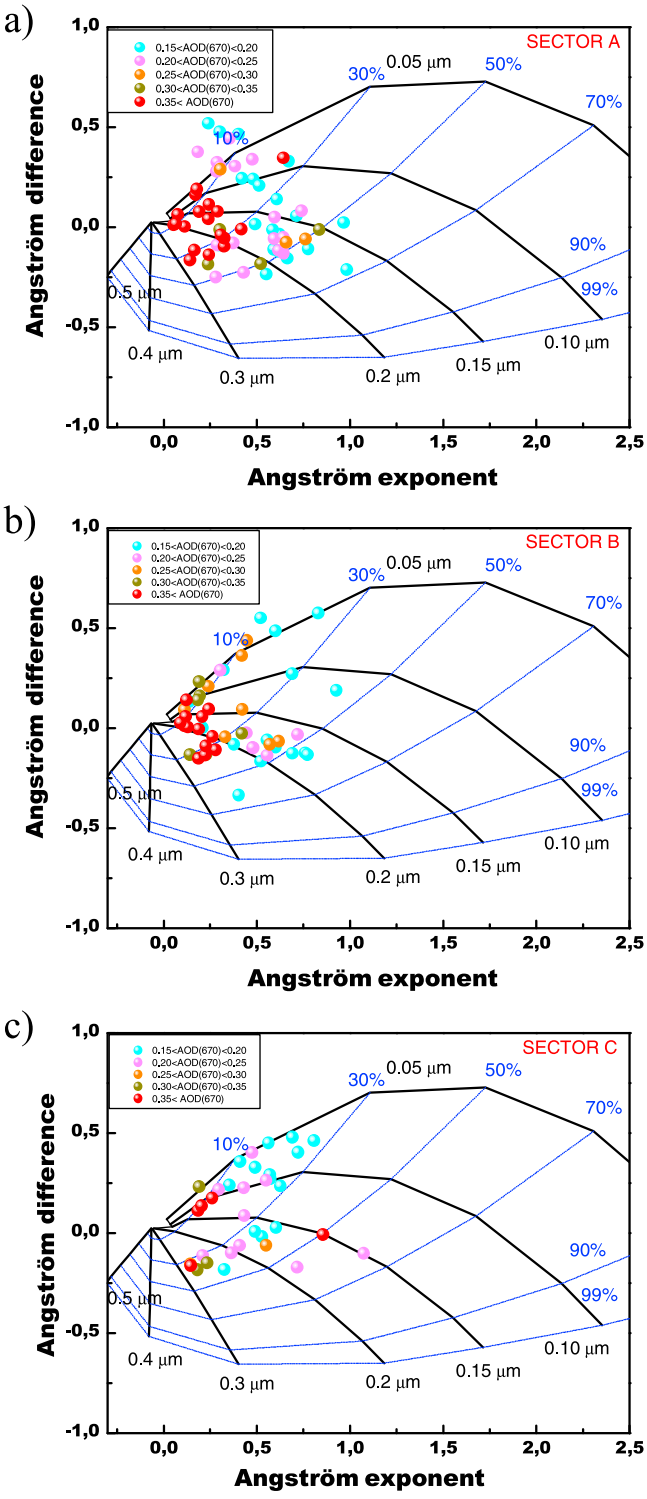

Figure 5. Angström exponent difference, $\delta\alpha = \alpha(440,670) - \alpha(670,870)$, as a function of α (440–670) and AOD (670 nm) for (a) sector A, (b) sector B, and (c) sector C.

from sector B toward Iberian Peninsula. This fact may explain the high mean value of AOD (440 nm) and the low mean value of α for sector B.

[25] The large standard deviations of the mean AOD values within of each sector origin (Table 1) indicate a large variability in the atmospheric aerosol load during desert dust events. This large variation could be related to several factors such as different meteorological conditions and the interactions of the desert dust with other pollutants which can modify their physical and chemical properties, such as chemical composition, morphology or hygroscopicity occurring during dust transport. The AOD and α values obtained in this study for each sector are coherent with the values reported by other authors analyzing desert dust events, and by the data recorded at AERONET sites influenced by desert dust. As example, *Lyamani et al.* [2005], using Sun photometer data, analyzed a Saharan dust outbreak during summer 1998 at Granada (Spain). These authors have reported values of AOD (500 nm) ranging from 0.20 to 0.6 and values of α in the range 0.36–0.37. *Prats et al.* [2008] reported mean values of AOD (440 nm) and α (440–870 nm) of 0.40 $\pm$ 0.23 and 0.45 $\pm$ 0.26, respectively, at El Arenosillo (Spain) during the dust intrusion events in summer 2004. At this same location, *Toledano et al.* [2007a] have obtained during other desert dust events a mean AOD (440 nm) value of 0.33 and mean α value of 0.52 for the 2000–2005 period. *El-Askary et al.* [2009] obtained an average value of 0.82 for AOD (675 nm) and 0.08 for α (440–675 nm) in the Alexandria (31.14°N, 29.59°E), Egypt, for a desert dust intrusion event. Nevertheless, these authors have reported AOD and α values similar to the obtained here for a mixture episode of desert dust and anthropogenic aerosol; AOD (675 nm) and α (440–675 nm) mean values of 0.37 and 0.44, respectively. The differences in these values compared to those obtained in our study could be due to differences related to the different measurement period (there is an inter-annual variability in the desert dust intrusions) and different pathways of the desert dust air masses during the transportation until the different stations.

[26] According to our results, the small difference in aerosol optical properties encountered between the different sectors classes appear to be not sufficient to help to discriminate the mineral dust optical properties from different source areas, except for sector B.

[27] To take more insight on the contribution of coarse dust particles to AOD, we have applied the method proposed by *Gobbi et al.* [2007] to our classification by sectors. This method gives us a first approximation of the fine mode fraction (η) as well as fine modal radius (R_f) and allows us to quantify the contribution of desert dust to AOD with no need of inversion. We have used the AOD (670 nm) to classify the aerosol properties as a function of α (440–870 nm) and its spectral curvature, represented by $\delta\alpha = \alpha(440,670) - \alpha(670,870)$.

[28] The results of Gobbi classification for the three sectors are shown in Figure 5. According to the recommendation of *Gobbi et al.* [2007], we have used in our study daily mean values of AOD (670 nm) > 0.15, in order to avoid errors in α larger than 30%. AOD values below 0.15 caused great uncertainty in the determination of the Angstrom exponent. Nevertheless, our study is focused on situations dominated by desert dust. Therefore, the bias introduced by the AOD > 0.15 filter is not expected to be so relevant (~5%). As shown in Figure 5, in up to 90% of data the coarse mode contribution to the AOD was always >50% for the three sectors. Angström parameter remained usually below 1. *Kaufman* [1993] established that strong negative

Table 2. Mean Volume Size Distribution Parameters for the Different Origin Sectors and Cluster Analysis[a]

	V_c ($\mu m^3/\mu m^2$)	r_c (μm)	V_f ($\mu m^3/\mu m^2$)	r_f (μm)	η (0.5 μm)
Sector A	0.17 ± 0.14	2.74 ± 1.49	0.015 ± 0.009	0.20 ± 0.03	0.34 ± 0.11
Sector B	0.16 ± 0.09	2.04 ± 1.37	0.015 ± 0.006	0.21 ± 0.03	0.29 ± 0.11
Sector C	0.13 ± 0.09	2.05 ± 1.11	0.014 ± 0.004	0.20 ± 0.03	0.36 ± 0.12
Cluster 1, 1500 m	0.16 ± 0.11	2.21 ± 1.24	0.015 ± 0.005	0.21 ± 0.03	0.32 ± 0.11
Cluster 2, 1500 m	0.15 ± 0.14	2.58 ± 1.44	0.014 ± 0.010	0.20 ± 0.03	0.33 ± 0.10
Cluster 1, 3000 m	0.17 ± 0.09	2.29 ± 1.23	0.015 ± 0.006	0.21 ± 0.04	0.30 ± 0.11
Cluster 2, 3000 m	0.15 ± 0.10	2.55 ± 1.44	0.016 ± 0.008	0.20 ± 0.03	0.34 ± 0.10

[a] V_c and V_f are the columnar volume of coarse and fine mode, respectively; r_c and r_f are modal radius at coarse and fine mode, respectively; and η is the fine mode fraction in 0.5 μm.

values of $\delta\alpha$ ranging from -0.5 to -0.3 indicate the dominance of aerosol fine mode. *Basart et al.* [2009] found that under the dominance of coarse aerosol particles, such as desert dust, $\delta\alpha$ tends to be negative or slightly positive with values in the range $(-0.3, 0.1)$. Values of $\delta\alpha$ larger than 0.1 indicate the contribution of fine mode fraction and coarse mode fraction to the calculation of AOD.

[29] Sector A showed AOD (670 nm) values above 0.25 in the 55% of cases, with $\delta\alpha$ varying from -0.15 to 0.45 (Figure 5a). This result suggests the possible existence of two situations: first, one dominated by coarse particles, and other one associated with the mix of both coarse and fine particles. High extinction values (AOD at 670 nm > 0.3) were found up to 45% of days for sector B which are often related to the presence of the coarse mode particles with $\alpha < 0.5$ and $\eta < 40\%$. In this sector, we found two predominant situations: (1°) $30\% \le \eta \le 50\%$ and $0.15 < R_f < 0.3$ μm, and (2°) $\eta < 30\%$ and $0.05 \le R_f \le 0.2$ μm. In the first situation, the values of $\delta\alpha$ slightly negative or close to zero indicate the most contribution of coarse mode fraction to the AOD. In the second situation, the cases with $\delta\alpha \ge 0.1$ indicate the presence of two separate particles modes related to dust particles mixed with fine anthropogenic particles. Sector C presented two well-defined sets of daily mean values. The first one with $30\% \le \eta \le 50\%$, $0.15 \le R_f$ and $\delta\alpha \le 0$, which is indicative that the main contribution to the calculation of AOD is the coarse mode fraction. The second one $\eta \le 30\%$ and $0.05 < R_f \le 0.3$ μm with $\delta\alpha \ge 0.1$ and indicates a fine mode and coarse mode contribute to the calculation of AOD (Figure 5c). *Basart et al.* [2009], based on AERONET data for the period 1994–2007 and applying the graphical method of *Gobbi et al.* [2007], performed an aerosol characterization for different Mediterranean areas (including the Iberian Peninsula). The result obtained in our study reveals a good agreement with the work of *Basart et al.* [2009] for the southeastern Iberian Peninsula. Both studies showed that the coarse mode normally appears mixed with other types of small particles as indicated by positive $\delta\alpha$ values.

4.1.1. Aerosol Volume Size Distribution

[30] In all sectors the aerosol volume size distributions exhibited two well defined modes (Table 2). The volume concentration and modal radius of the fine mode showed similar mean values for the three origin sectors (volume concentration around 0.015 ± 0.009 $\mu m^3/\mu m^2$ and fine mode radius around 0.20 ± 0.03 μm). These results indicate that the fine mode was independent of the sector origin. Thus, this mode could be related to the anthropogenic aerosol produced locally or transported from polluted areas in European continent and of the most industrialized areas of the North Africa coast. *Olmo et al.* [2006] have obtained the same value of fine mode volume concentration (V_f) when our station was affected by Saharan air masses and during polluted episodes (0.020 ± 0.007 $\mu m^3/\mu m^2$). Thus, the results suggest that the dust transport to our study area could be accompanied by the transport of anthropogenic particles from industrialized areas in North Africa. In this sense, *Rodriguez et al.* [2011] established that the main industrial emissions in this region occur along the Atlantic coast of Morocco, northern Algeria, eastern Algeria and Tunisia. Additionally, during the SAMUM 2006 campaign, *Kaaden et al.* [2009] found that the smallest aerosol particles were probably anthropogenic back-ground aerosol. *Prats et al.* [2008] showed that the fine mode volume concentration during desert dust days increased with respect to dust-free days at El Arenosillo, indicating that the intrusions of desert dust aerosol contributed to the fine mode in this station. *Fu et al.* [2010] studied the impact of dust events on the air quality and demonstrated the mixing characteristics of dust aerosol with anthropogenic pollution along the transport pathway from the deserts to the northern cities in China.

[31] On the other hand, we have also computed the ratio between the coarse and fine volume concentrations (V_c/V_f). For all sectors, the mean value of the ratio V_c/V_f shows the dominance of coarse mode particles during desert dust events, being more pronounced for sectors A and B with mean value of 11 ± 6. In sector C a mean value of 9 ± 5 was obtained for V_c/V_f. The V_c/V_f ratios up to about 15 were retrieved at Lampedusa by *Tafuro et al.* [2006]. The difference between the V_c/V_f ratios of Lampedusa and the ratios obtained in our study site may be due to differences in dust load and sedimentation effects that reduce the contribution of large particles as well as to the difference in the local aerosol anthropogenic contribution.

4.1.2. Single Scattering Albedo and Asymmetry Parameter

[32] The most important feature of $\omega_0(\lambda)$ for all sectors (Figure 6) was its spectral variation (slight increase with wavelength) as shown in other studies for desert dust events [e.g., *Collaud Coen et al.*, 2004; *Lyamani et al.*, 2006; *Alados-Arboledas et al.*, 2008; *Cachorro et al.*, 2008; *Su and Toon*, 2011; *Toledano et al.*, 2011]. The increase of $\omega_0(\lambda)$ with wavelength is a typical pattern for dust [*Eck et al.*, 2010] due to the spectral absorption properties of iron oxides in dust [*Sokolik and Toon*, 1999]. Although the differences in $\omega_0(\lambda)$ values obtained for the three sectors are in the range of the standard deviations, it can be seen that the high mean values were found for sector B and C, ranging

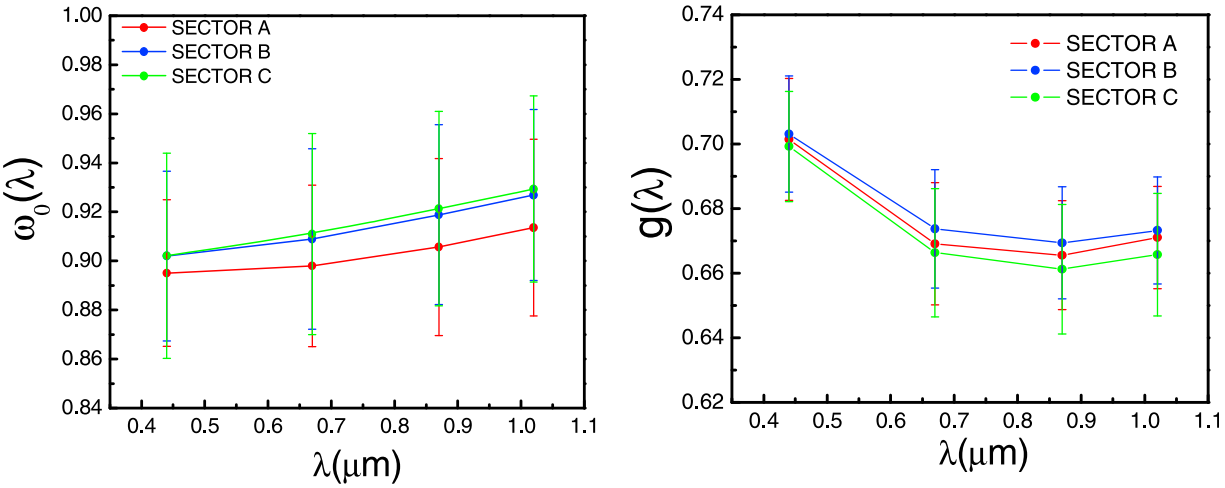

Figure 6. The single scattering albedo and asymmetry parameter according to the classification by origin sectors.

from 0.90 ± 0.03 at 440 nm to 0.93 ± 0.03 at 1020 nm. The slightly lower mean $\omega_0(\lambda)$ values were found for sector A at all wavelengths, ranging from 0.89 ± 0.03 at 440 nm to 0.91 ± 0.03 at 1020 nm. To corroborate the $\omega_0(\lambda)$ values between different sectors, we have applied the Kolmogorov-Smirnov non-parametric test. On the one hand, this test revealed, at the 95% confidence level, that mean $\omega_0(\lambda)$ values at all wavelengths at the sector A are significantly different with respect the $\omega_0(\lambda)$ values at all wavelengths at the sectors B and C. On the other hand, the same test revealed that the $\omega_0(\lambda)$ values at all wavelengths from sector B and C are not significantly different.

[33] *Kim et al.* [2011] obtained mean $\omega_0(\lambda)$ values between 0.90 and 0.94 at 440 nm in Tamanrasset (center of the Saharan desert). The lower $\omega_0(\lambda)$ mean values obtained in our study compared to those retrieved by other authors may be due to local urban contribution and aerosol mixtures during the dust transport. Several works [e.g., *Lyamani et al.*, 2006, 2010; *Perrone and Bergamo*, 2011; *Rodríguez et al.*, 2011] have reported that the contribution of anthropogenic particles could be significant during desert dust events over sites several hundred km off North Africa. *Mladenov et al.* [2011] showed that Saharan dust is an important source of anthropogenic matter during desert events detecting at the remote observatory at the Sierra Nevada monitoring station (OSN). During those same desert dust events, columnar aerosol data were retrieved in the Granada city (Spain). Mean daily $\omega_0(\lambda)$ ranged from 0.89 ± 0.03 at 440 nm to 0.92 ± 0.03 at 1020 nm. These values are in accordance with the mean values obtained in our study. Additionally, *Tafuro et al.* [2006] have also obtained a low mean value of 0.89 ± 0.03 at 440 nm at Lampedusa (a small Italian island located about 130 km east of the coasts of Tunisia), during desert dust events. These results highlight the great influence of the anthropogenic aerosol in the Mediterranean area. Numerous studies based on the chemical composition of the ground-collected particulate matter (PM) have revealed the significant role of anthropogenic particles to the PM collected during dust intrusion events over Mediterranean areas as southeastern Italy [e.g., *Bellantone et al.*, 2008]. *Pereira et al.* [2011] established that during the influence of North African air masses, the scattering was dominated by fine particles indicating that either dust at the surface was not so frequent or that it was mixed with anthropogenic pollution.

[34] *Kaaden et al.* [2009] found that the Saharan aerosol at Tinfou (Morocco) consists of a combination of anthropogenic compounds (predominantly non natural sulphate and carbonaceous particles) and mineral dust. In situ measurements in the same station showed that during low dust concentration, ranged from 0.91 ± 0.02 at 537 nm to 0.93 ± 0.01 whereas the absorption could be explained by soot-type particles [*Schladitz et al.*, 2009]. *Müller et al.* [2009] showed that soot absorption is correlated with particles smaller than 550 nm in diameter and the dust absorption is correlated with particles larger than 550 nm during the SAMUM 2006 campaign.

[35] The mean values of asymmetry parameter (Figure 6) showed a little variation with wavelengths for the three sectors (0.67 ± 0.02). This result was similar to that obtained by *Olmo et al.* [2008] in Granada during desert dust events. The differences in $g(\lambda)$ values obtained in the three sectors were within the standard deviations. The Kolmogorov-Smirnov non-parametric test has been also applied to the mean $g(\lambda)$ values between the different sectors. This test revealed, at the 95% confidence level, that the differences in the mean $g(\lambda)$ values are no significant by three sectors.

4.2. Aerosol Properties Classification by Cluster Analysis

[36] In this section, we investigate the dependence of aerosol radiative properties on air mass pathways. During the analyzed desert dust events the air masses arriving at Granada at 500 m a.g.l. never passed over the North Africa continent. This suggests that the transport of desert dust occur mainly at higher level and vertical mixing as well as gravitational settling processes were responsible for the presence of desert dust particles near surface. *Tesche et al.* [2009] showed that the height that can reach the dust particles when they are injected to the atmosphere were up to 7 km during SAMUM campaign. *Papayannis et al.* [2008] performed more than 130 observation days of the

horizontal and vertical extent of Saharan dust intrusions over Europe by means of a coordinated lidar network in the frame of the European Aerosol Research Lidar Network (EARLINET). They found that Saharan dust source regions play a key role in the dust transport to Europe in the height region between 3 and 5 km. In addition, they analyze the main pathways of Saharan dust transport over Europe, founding that western Europe is mainly affected by the western Saharan region. In our analysis, we assumed that the trajectories ending at 1500 and 3000 m provide information on the transport of desert dust. The 1500 m level represents the interaction of the air masses trajectories with boundary layer over reception site while the 3000 m level represents of the air masses transport at the free troposphere. The cluster analysis resulted in two groups or clusters of back-trajectories for African air masses arriving at Granada at 1500 and 3000 m levels. Flow patterns were different at each level (Figure 7). Each level had a distinctive set of mean flow patterns that represents clusters of back-trajectories. The difference between this type of classification and the classification by sector origin is that the cluster method groups together the back-trajectories with similar lengths and same curvature. The trajectories grouped in cluster 1 at 1500 m level came from northern Algeria and correspond to 44% of the trajectories in this level arriving from North African. Its mean length was 1370 km. The air masses transport according to the pathway of cluster 1 was favored in the most cases with high pressure system (at level 850 hPa) centered over Mediterranean sea associated with a low pressure over Morocco. This meteorological scenario favored the desert dust transport toward the southeast of the Iberian Peninsula across the north Algeria. According to this scenario, the dust sources should be north of Algeria, Tunisia and northeastern Morocco. At 1500 m level the trajectories grouped in cluster 2 (56% of cases) were associated in the most cases with low pressures (observed from sea level to 850 hPa) centered southwest Portugal coast (Figure 9). This situation is coincident with one of the main synoptic sceneries that permit the air masses transport from North Africa toward Iberian Peninsula established by *Escudero et al.* [2005]. Source areas of mineral dust should vary widely but according to the transport scenario, Western regions of Morocco should be the main emission sources areas. At 3000 m level, the trajectories tended to be longer, indicating greater wind speeds. The two clusters at 3000 m level showed more curvature than the 1500 m level clusters. The meteorological scenario associated with cluster 1 was caused in the most cases by the intense ground heating in the Sahara region during the summer months enhances atmospheric convection, favoring dust injection at high altitudes up to 5000 m a.s.l. [*Prospero and Carlson*, 1972]. The dust layer is transported at these altitudes by a compensatory high-pressure center (Figure 9). The surface low pressures (figure not shown) were located over northwestern Africa while the high pressures (at level 700 hPa) were located over North Africa and the south of the Iberian Peninsula. According to this scenario, the dust sources should be southwestern Algeria, northern Mauritania and western Sahara. This cluster grouped 46% of the trajectories in this level. Its mean length was of 2049 km. The most frequent synoptic situation related to the trajectories associated with cluster 2 was caused by low pressure located in front of the south Portugal coast (at level 700 hPa) associated with a high pressure located in the interior of North Africa at the same level (Figure 9). At the surface level, a low pressure (figure not shown) may permit the injection of dust at high levels. This meteorological scenario could favor the air masses transport from North Africa toward the Iberian Peninsula. This cluster grouped 54% of the trajectories. Its length was the longest with a mean value of 2393 km. The air masses trajectories along with their cluster-mean for 1500 and 3000 m levels are shown in Figure 7. Table 3 shows the main synoptic scenarios that favored the North Africa air masses transport toward the southeastern of the Iberian Peninsula. The synoptic scenario that has a higher frequency was the low Atlantic pressure and high Mediterranean Sea pressure or northeast Africa. The second synoptic scenario in frequency distribution was a high pressure over northern African continent that favored the air masses transport from western Saharan desert. Finally, another relevant synoptic scenario was low pressure over Morocco and high pressure over northeast Africa.

[37] Annual frequencies of air masses assigned to each cluster at each level are show in Figure 8. At 1500 m level grouped 67% of air masses from North Africa, cluster 1 (northern Algeria) showed maximum frequency in May–August and cluster 2 in July–August. The classification at 3000 m level grouped 33% of air masses from North Africa. In this level, cluster 1 showed two maxima during annual evolution, in May and July. Cluster 2 grouped air masses which arrived between June and October.

[38] Table 1 shows the statistical summary of AOD (440 nm) and α (440–1020 nm) according to the cluster classification. At the 1500 m level, the air masses transported from northern Algeria Tunisia and northeastern Morocco which have been grouped in cluster 1 (Figure 9) had a higher mean value of AOD (440 nm) (0.29 ± 0.14) than cluster 2 (0.24 ± 0.16). In addition, the histograms of relative frequency of both variables are shown in Figure 10.

[39] The slightly higher value of AOD (440 nm) for cluster 1 than for cluster 2 could be due to the large time travel and the slow movement of the air masses in cluster 1 over mineral dust sources in comparison with cluster 2. Moreover, α (440–1020 nm) presented a lower mean value for cluster 1 than for cluster 2 with mean values of 0.39 ± 0.20 and 0.44 ± 0.21, respectively. Therefore, cluster 1 showed a higher proportion of coarse particles than cluster 2. At 3000 m level, the AOD (440 nm) for cluster 1 showed a higher mean value than cluster 2 with 0.29 ± 0.13 and 0.26 ± 0.16, respectively, and α (440–1020 nm) presented a lower value for cluster 1 (0.38 ± 0.20) than for cluster 2 (0.45 ± 0.19). These results can be justified by the longer travel time over mineral dust sources of air masses assigned to cluster 1.

[40] The results using the *Gobbi et al.* [2007] method for all clusters (figures not shown) shows that in up to 90% of observations the fine mode fraction was <50%. However, this mode was always present during desert dust intrusions which could be related with anthropogenic aerosol contribution. High extinction values (AOD (670 nm) > 0.4) were found for cluster 1 at 1500 m and 3000 m levels which are often related with the presence of dust particles with $\alpha < 0.5$

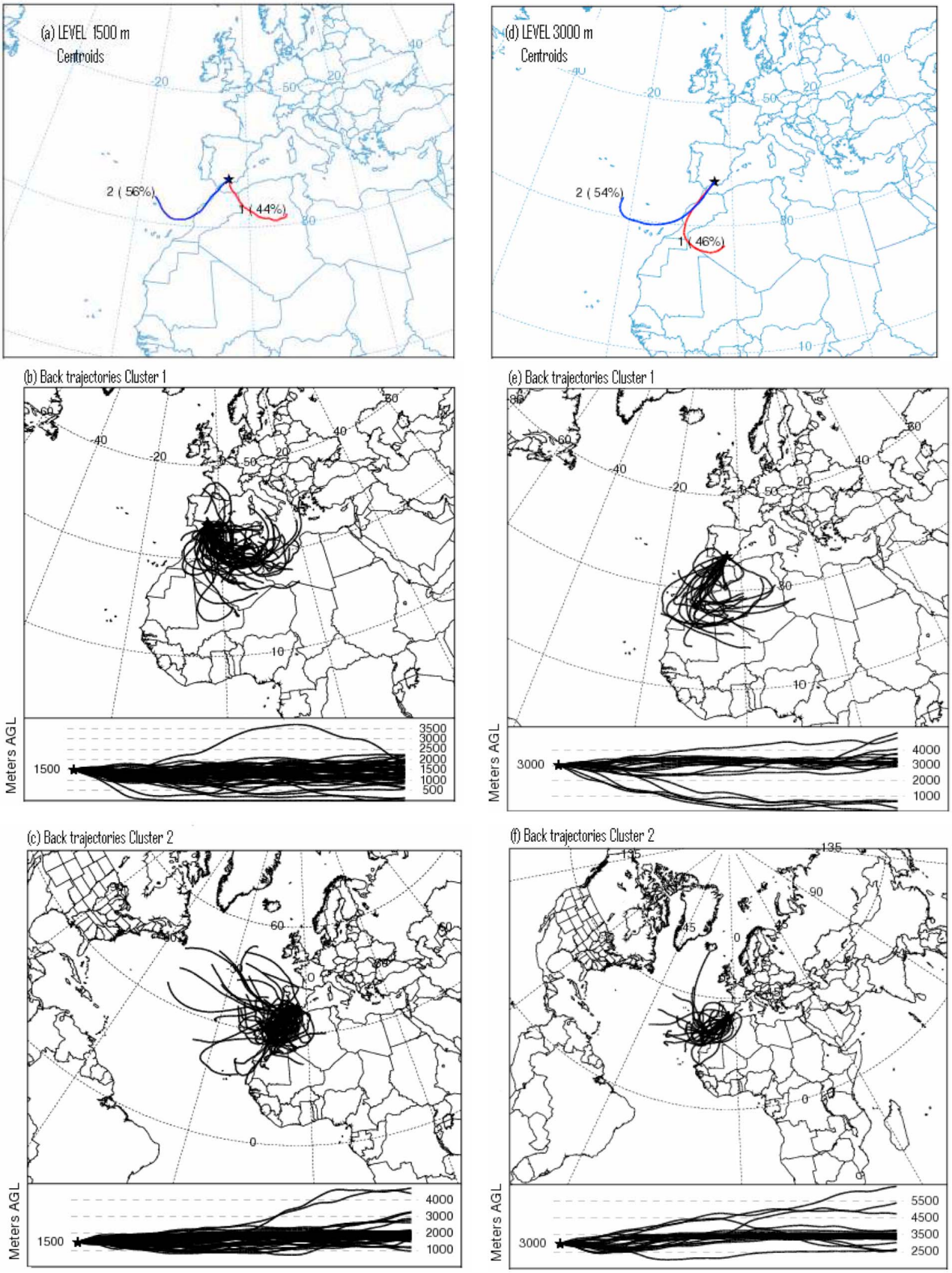

Figure 7. Centroids of cluster classification at (left) 1500 m level, and (right) 3000 m level.

Table 3. The Main Synoptic Scenarios That Favored Air Mass Transport From North Africa Toward the Iberian Peninsula From the 2005–2010 Period

	Sector Sources Origin	Cluster Analysis
Low-pressure Atlantic and high-pressure Mediterranean Sea or northeast Africa	sector A (47%)	cluster 2 (56%) at the 1500 m level; cluster 2 (54%) at the 3000 m level
Low pressure over Morocco and high pressure over northeast Africa	sector C (22%)	cluster 1 (44%) at the 1500 m level
High pressure over northern African continent	sector B (31%)	cluster 1 (46%) at the 3000 m level

and $\delta\alpha \sim 0$. We could found for all clusters high AOD (670 nm) values combined with low α in two situations: 1°) $\eta <$ 40% and $R_f \sim 0.2$ μm, and 2°) $\eta < 30\%$ and $R_f \sim 0.12$ μm. In the first case, the cases with $\delta\alpha \sim 0$ indicate the predominance of one mode associated to coarse dust particles. En the second case, the cases with $\delta\alpha \geq 0.1$ indicate the presence of two separate particles modes, related with dust mixed with fine anthropogenic particles.

4.2.1. Aerosol Volume Size Distribution

[41] The volume size distribution was found to be bimodal. The size distribution parameters are shown in Table 3. The volume concentration (V_f) and modal radius (r_f) of the fine mode showed small variations for all the clusters with mean values of V_f between 0.014 ± 0.010 $\mu m^3/\mu m^2$ and 0.016 ± 0.008 $\mu m^3/\mu m^2$ and mean value of r_f close to 0.20 ± 0.03 μm. The fine mode was independent of the height and speed of the air masses transport from North Africa and it could be related to local emissions or anthropogenic aerosol transport from the Mediterranean areas [*Lyamani et al.*, 2006]. On the other hand, the volume concentration (V_c) and modal radius (r_c) of the coarse mode showed a large standard deviation within the different clusters. At 1500 m level, cluster1 had a mean V_c of 0.16 ± 0.11 $\mu m^3/\mu m^2$ with the center of the peak in 2.21 ± 1.24 μm while cluster 2 had a mean V_c of 0.15 ± 0.14 $\mu m^3/\mu m^2$ with the center of the peak in 2.58 ± 1.44 μm. This large variation could be related to the interactions of the desert dust with other aerosol types occurring during dust transport.

[42] At 3000 m level, cluster1 showed a higher V_c with a mean value 0.17 ± 0.09 $\mu m^3/\mu m^2$ and the center of the peak in 2.29 ± 1.23 μm compared with the values found at 1500 m level, while for cluster 2 a mean value of V_c of 0.15 ± 0.10 $\mu m^3/\mu m^2$ with the center of the peak in 2.55 ± 1.44 μm was found. At 1500 m level the mean value of the ratio V_c/V_f was 11 ± 6 for both clusters, indicating the dominance of coarse mode particles during desert dust events. At 3000 m level V_c/V_f was 11 ± 6 for cluster 1 and 10 ± 5 for cluster 2. The results given by *Tafuro et al.* [2006] at the Lampedusa Island (V_c/V_f ratio of 15) are not in accordance with the results shown in our work. This difference may be due to three reasons: (1) differences related to the different measurement period (there is an inter-annual variability in the desert dust intrusions), (2) differences related to the different of the desert dust intrusions detection method, and (3) different pathways of the desert dust air masses during the transport until the two stations.

4.2.2. Single Scattering Albedo and Asymmetry Parameter

[43] During desert dust events $\omega_0(\lambda)$ showed slight spectral dependence increasing with wavelength for all the clusters (Figure 11). In cluster 1 $\omega_0(\lambda)$ ranged from 0.90 ± 0.03 at 440 nm to 0.93 ± 0.03 at 1020 nm, while in cluster 2 this parameter ranged from 0.89 ± 0.03 at 440 nm to 0.92 ± 0.03 at 1020 nm. At 1500 m level, cluster 1 showed slightly higher values of $\omega_0(\lambda)$ than cluster 2, indicating that probably the air masses in the last cluster transported more absorbing particles. Air masses grouped into cluster 2 passed mainly over the indusial areas in Atlantic coast of Morocco where desert dust could be mixed with anthropogenic particles emitted in these areas. At 3000 m level, cluster 1 and 2 showed similar mean values of $\omega_0(\lambda)$.

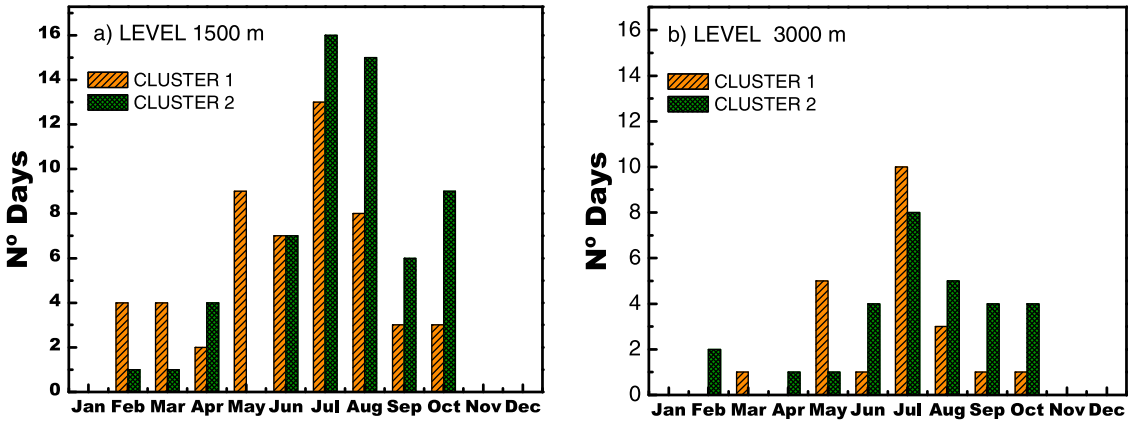

Figure 8. Monthly frequency of African air masses according to the cluster analysis at (a) 1500 m and (b) 3000 m.

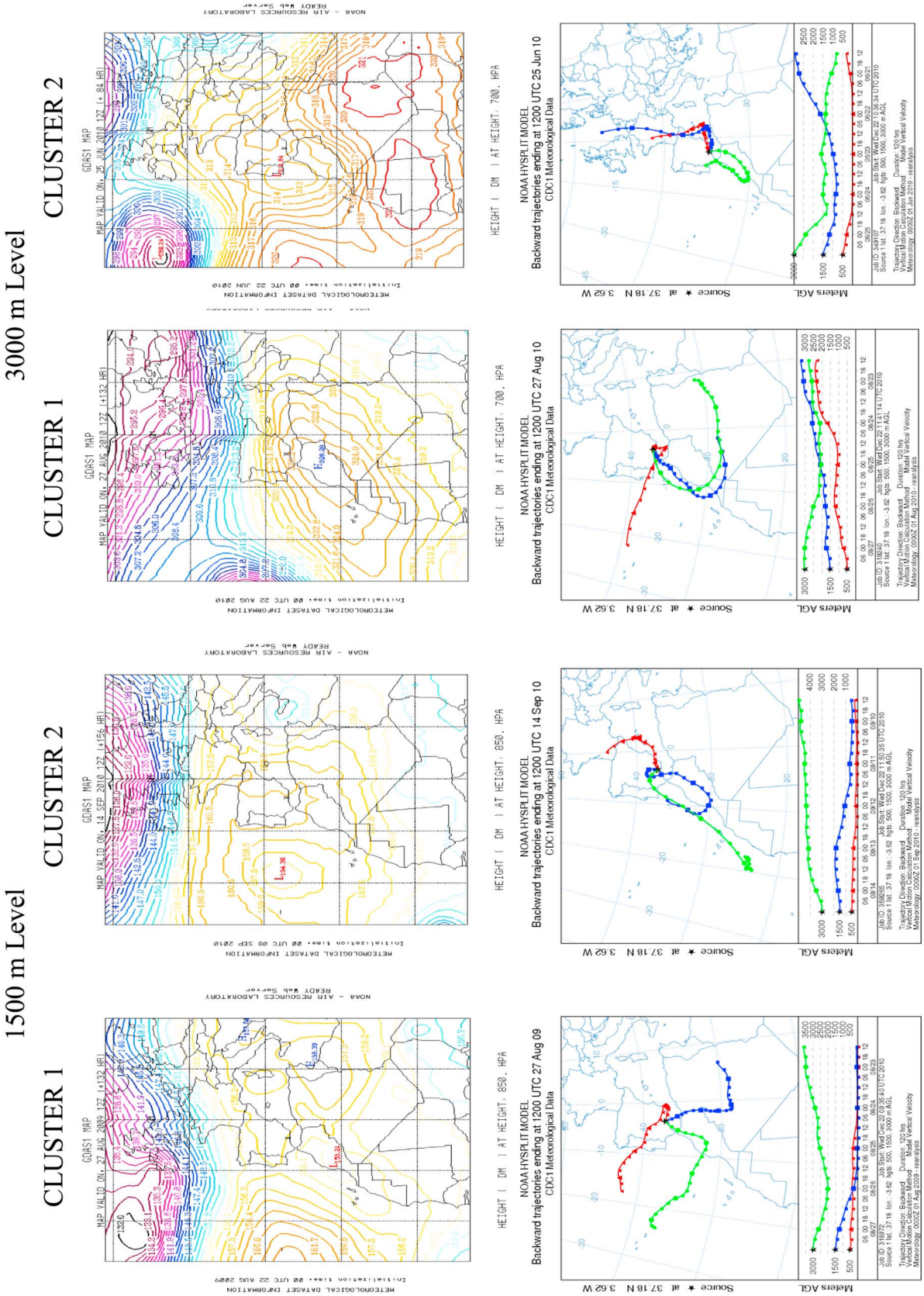

Figure 9. The main synoptic sceneries and back-trajectories at the 500, 1500, and 3000 m levels according to the cluster analysis.

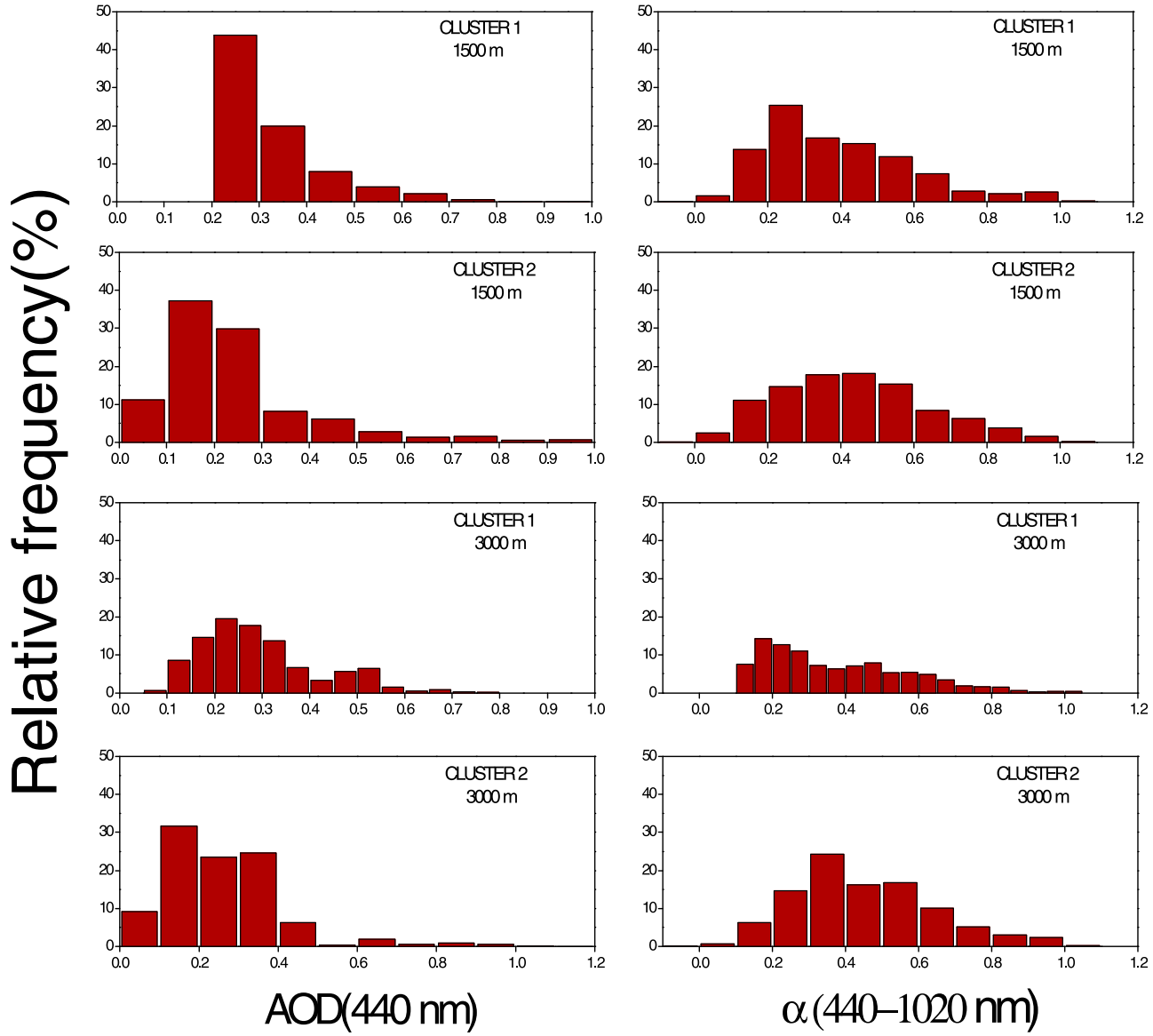

Figure 10. Frequency distribution of AOD (440 nm) and α (440–1020 nm) according to the cluster analysis.

[44] On the other hand, as in the classification by origin sectors, the mean values of $g(\lambda)$ showed similar values (0.67 ± 0.02) with wavelengths for all the clusters (Figure 11).

5. Conclusions

[45] Some relevant conclusions may be drawn from the study of the aerosol optical and microphysical properties by sector origin and cluster analysis during desert dust events recorded at Granada (Spain) from January 2005 to December 2010. Both classification methods agree in that the air masses transport from North Africa toward the southeastern of the Iberian Peninsula follow three main pathways; either from northern Algeria and Tunisia, northern Morocco and over the Sahara region. The two methods also show that the aerosol optical and microphysical properties during North Africa desert dust over Granada have a weak dependence on the sources origin and pathways. Nevertheless, significant differences are found when air masses are transported from the Sahara area (sector B and cluster 1 at the 3000 m level). The larger mean value of AOD (440 nm) and lower mean value of α (440–1020 nm) are successfully identified by both methods.

[46] Additionally, the sectors methodology and the clusters analysis are in accordance with the slightly lower $\omega_0(\lambda)$ values obtained when air masses are transported from the north of Morocco area (sector A and cluster 2 in the 1500 m level). This result may be probably due to the mixing of desert dust with absorbing pollutants from North African industrial areas. Nevertheless, for the three sectors, $\omega_0(\lambda)$ was lower than the values obtained at others locations during desert dust events. This result points out the strong contribution of local anthropogenic aerosol and polluted transported from Mediterranean areas at Granada.

[47] The sectors classification and clusters analysis showed that Granada was affected during desert dust

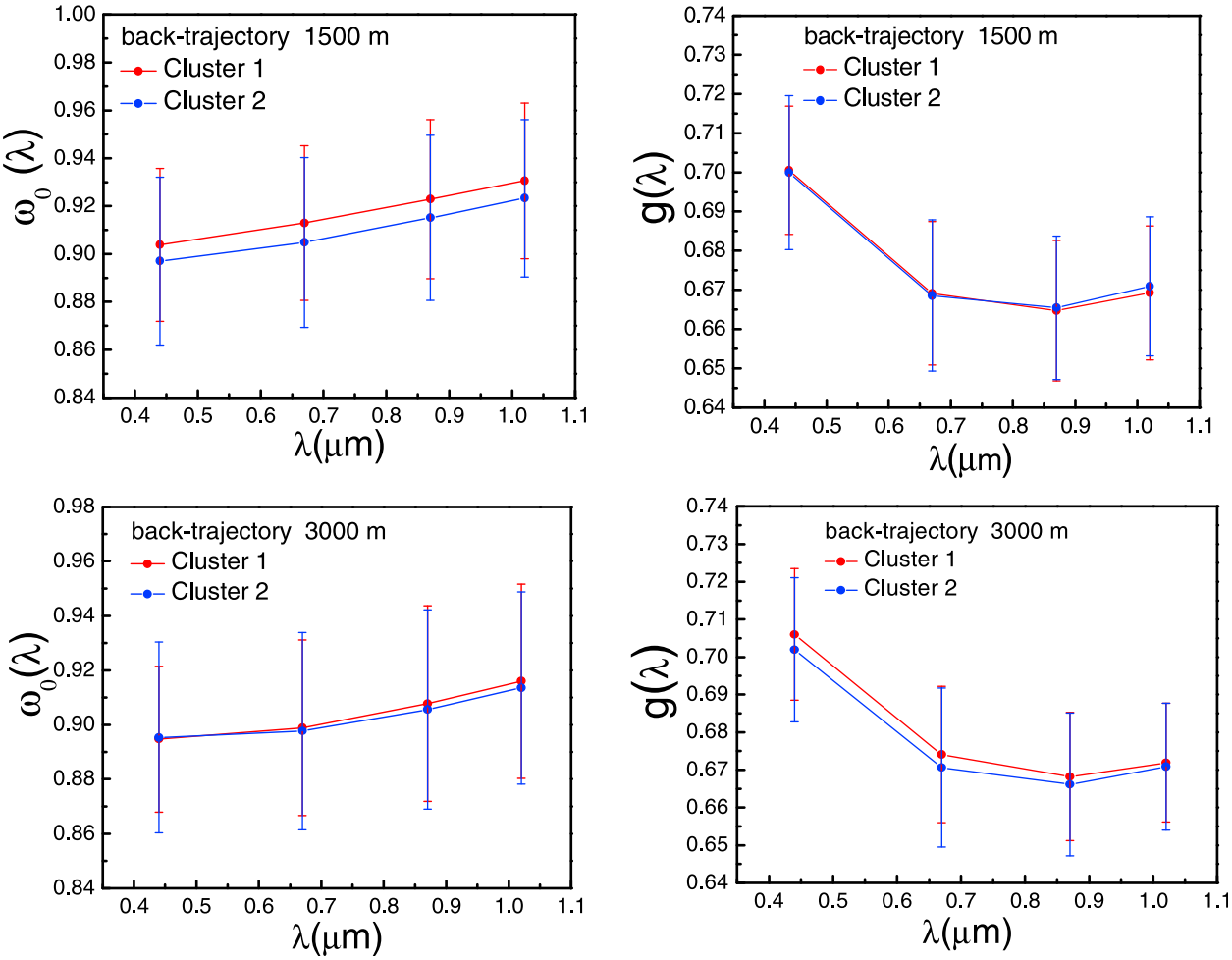

Figure 11. The single scattering albedo and asymmetry parameter according to the cluster analysis.

intrusions by two particle size modes, where the coarse mode was the dominating mode according to the V_c/V_f ratio values.

[48] All these results can help us to constrain uncertainties in estimating global dust radiative forcing. In future works, we will use the aerosol radiative properties obtained in our analyses for study the aerosol forcing impact in areas like southern Spain during desert dust intrusions taking account the air mass classification.

[49] **Acknowledgments.** This work was supported by the Andalusia Regional Government through projects P08-RNM-3568 and P10-RNM-6299; by the Spanish Ministry of Science and Technology through projects CGL2008-01330-E/CLI (Spanish Lidar Network), CGL2010–18782, and CSD2007–00067; and by EU through ACTRIS project (EU INFRA-2010-1.1.16–262254). We acknowledge the NOAA Air Resources Laboratory (Russell et al.) for the use of HYSPLIT model. We would like express their gratitude to the CALIMA project.

References

Alados-Arboledas, L., H. Lyamani, and F. J. Olmo (2003), Aerosol size properties at Armilla, Granada (Spain), *Q. J. R. Meteorol. Soc.*, *129*, 1395–1413, doi:10.1256/qj.01.207.

Alados-Arboledas, L., et al. (2008), Aerosol columnar properties retrieved from CIMEL radiometers during VELETA 2002, *Atmos. Environ.*, *42*, 2654–2667, doi:10.1016/j.atmosenv.2007.10.006.

Basart, S., C. Perez, E. Cuevas, J. M. Baldasano, and G. P. Gobbi (2009), Aerosol characterization in Northern Africa, Northeastern Atlantic, Mediterranean Basin and Middle East from direct-sun AERONET observations, *Atmos. Chem. Phys.*, *9*, 8265–8282, doi:10.5194/acp-9-8265-2009.

Bauer, S., E. Bierwirth, M. Esselborn, A. Petzold, A. Macke, T. Trautmann, and M. Wendisch (2011), Airborne spectral radiation measurements to derive solar radiative forcing of Saharan dust mixed with biomass burning smoke particles, *Tellus, Ser. B*, *63*, 742–750.

Bellantone, V., I. Carofalo, F. De Tomasi, M. R. Perrone, M. Santese, A. M. Tafuro, and A. Turnone (2008), In situ samplings and remote sensing measurements to characterize aerosol properties over South-East Italy, *J. Atmos. Oceanic Technol.*, *25*(8), 1341–1356, doi:10.1175/2007JTECHA958.1.

Bond, T. C., and R. W. Bergstrom (2006), Light absorption by carbonaceous particles: An investigative review, *Aerosol Sci. Technol.*, *40*, 27–67, doi:10.1080/02786820500421521.

Bösenberg, J., et al. (2003), A European aerosol research lidar network to establish an aerosol climatology, *MPI Rep., 348*, Max-Planck-Inst. für Meteorol., Hamburg, Germany.

Cachorro, V. E., C. Toledano, N. Prats, M. Sorribas, S. Mogo, A. Berjón, B. Torres, R. Rodrigo, J. de la Rosa, and A. M. De Frutos (2008), The strongest desert dust intrusion mixed with smoke over the Iberian Peninsula registered with Sun photometry, *J. Geophys. Res.*, *113*, D14S04, doi:10.1029/2007JD009582.

Collaud Coen, M., E. Weingartner, D. Schaub, C. Hueglin, C. Corrigan, S. Henning, M. Schwikowski, and U. Baltensperger (2004), Saharan dust events at the Jungfraujoch: Detection by wavelength dependence of the single scattering albedo and first climatology análisis, *Atmos. Chem. Phys.*, *4*, 2465–2480, doi:10.5194/acp-4-2465-2004.

Córdoba-Jabonero, C., et al. (2011), Synergetic monitoring of Saharan dust plumes and potential impact on surface: A case study of dust transport from Canary Islands to Iberian Peninsula, *Atmos. Chem. Phys.*, *11*, 3067–3091, doi:10.5194/acp-11-3067-2011.

Dorling, S. R., T. D. Davies, and C. E. Pierce (1992), Cluster analysis: A technique for estimating the synoptic meteorological controls on air and precipitation chemistry—Results from Eskdalemuir, south Scotland, *Atmos. Environ.*, *26*, 2583–2602.

Draxler, R. R., and G. D. Hess (1998), An overview of the HYSPLIT_4 modelling system for trajectories, dispersion and deposition, *Aust. Meteorol. Mag.*, *47*, 295–308.

Draxler, R. R., and G. Rolph (2003), HYSPLIT (Hybrid Single-Particle Lagrangian Integrated Trajectory) Model, NOAA Air Resour. Lab., Silver Spring, Md. [Available at http://www.arl.noaa.gov/ready/hysplit4.html.]

Draxler, R. R., B. Stunder, G. Rolph, and A. Taylor (2009), *HYSPLIT_4 User's Guide*, NOAA Air Resour. Lab., Silver Spring, Md.

Dubovik, O., B. Holben, T. F. Eck, A. Smirnov, Y. J. Kaufman, M. D. King, D. Tanre, and I. Slutsker (2002a), Variability of absorption and optical properties of key aerosol types observed in worldwide locations, *J. Atmos. Sci.*, *59*, 590–608, doi:10.1175/1520-0469(2002)059<0590:VOAAOP>2.0.CO;2.

Dubovik, O., B. N. Holben, T. Lapyonok, A. Sinyuk, M. I. Mishchenko, P. Yang, and I. Slutsker (2002b), Non-spherical aerosol retrieval method employing light scattering by spheroids, *Geophys. Res. Lett.*, *29*(10), 1415, doi:10.1029/2001GL014506.

Duran, P. (1997), Medidas espectrorradiométricas para la determinación de componentes atmosféricos (ozono, vapor de agua y aerosoles) y modelización del intercambio radiativo en la atmósfera, Ph.D. thesis, Univ. de Valladolid, Valladolid, Spain.

Eck, T. F., et al. (2010), Climatological aspects of the optical properties of fine/coarse mode aerosol mixtures, *J. Geophys. Res.*, *115*, D19205, doi:10.1029/2010JD014002.

El-Askary, H., R. Farouk, C. Ichoku, and M. Kafatos (2009), Transport of dust and anthropogenic aerosols across Alexandria, Egypt, *Ann. Geophys.*, *27*, 2869–2879, doi:10.5194/angeo-27-2869-2009.

Engelstaedter, S., I. Tegen, and R. Washington (2006), North African dust emissions and transport, *Earth Sci. Rev.*, *79*, 73–100, doi:10.1016/j.earscirev.2006.06.004.

Escudero, M., S. Castillo, X. Querol, A. Avila, M. Alarcón, M. M. Viana, A. Alastuey, E. Cuevas, and S. Rodríguez (2005), Wet and dry African dust episodes over eastern Spain, *J. Geophys. Res.*, *110*, D18S08, doi:10.1029/2004JD004731.

Escudero, M., A. F. Stein, R. R. Draxler, X. Querol, A. Alastuey, S. Castillo, and A. Avila (2011), Source apportionment for African dust outbreaks over the Western Mediterranean using the HYSPLIT model, *Atmos. Res.*, *99*, 518–527, doi:10.1016/j.atmosres.2010.12.002.

Estellés, V., et al. (2006), Intercomparison of spectroradiometers and Sun photometers for the determination of the aerosol optical depth during the VELETA-2002 field campaign, *J. Geophys. Res.*, *111*, D17207, doi:10.1029/2005JD006047.

Estellés, V., J. A. Martinez-Lozano, and M. A. P. Utrillas (2007), Influence of air mass history on the columnar aerosol properties at Valencia, Spain, *J. Geophys. Res.*, *112*, D15211, doi:10.1029/2007JD008593.

Fu, Q., et al. (2010), Source, long-range transport, and characteristics of a heavy dust pollution event in Shanghai, *J. Geophys. Res.*, *115*, D00K29, doi:10.1029/2009JD013208.

Garcia, O. E., F. J. Exposito, J. P. Diaz, and A. M. Diaz (2011), Radiative forcing under mixed aerosol conditions, *J. Geophys. Res.*, *116*, D01201, doi:10.1029/2009JD013625.

Gobbi, G. P., Y. J. Kaufman, I. Koren, and T. F. Eck (2007), Classification of aerosol properties derived from AERONET direct sun data, *Atmos. Chem. Phys.*, *7*, 453–458, doi:10.5194/acp-7-453-2007.

Goudie, A. S., and N. J. Middleton (2001), Saharan dust storms: Nature and consequences, *Earth Sci. Rev.*, *56*, 179–204, doi:10.1016/S0012-8252(01)00067-8.

Gu, Y., K. N. Liou, W. Chen, and H. Liao (2010), Direct climate effect of black carbon in China and its impact on dust storms, *J. Geophys. Res.*, *115*, D00K14, doi:10.1029/2009JD013427.

Guerrero-Rascado, J. L., F. J. Olmo, I. Avilés-Rodríguez, F. Navas-Guzmán, D. Pérez-Ramírez, H. Lyamani, and L. Alados Arboledas (2009), Extreme Saharan dust event over the southern Iberian Peninsula in September 2007: Active and passive remote sensing from surface and satellite, *Atmos. Chem. Phys.*, *9*, 8453–8469, doi:10.5194/acp-9-8453-2009.

Hand, V., G. Capes, D. Vaughan, P. Formenti, M. Jim, J. Haywood, and H. Coe (2010), Evidence of internal mixing of African dust and biomass burning particles by individual particle analysis using electron beam techniques, *J. Geophys. Res.*, *115*, D13301, doi:10.1029/2009JD012938.

Holben, B. N., et al. (1998), AERONET—A federated instrument network and data archive for aerosol characterization, *Remote Sens. Environ.*, *66*, 1–16, doi:10.1016/S0034-4257(98)00031-5.

Kaaden, N., et al. (2009), State of mixing, shape factor, number size distribution, and hygroscopic growth of the Saharan anthropogenic and mineral dust aerosol at Tinfou, Morocco, *Tellus, Ser. B*, *61*, 51–63, doi:10.1111/j.1600-0889.2008.00388.x.

Kandler, K., et al. (2009), Size distribution, mass concentration, chemical and mineralogical composition and derived optical parameters of the boundary layer aerosol at Tinfou, Morocco, during SAMUM 2006, *Tellus, Ser. B*, *61*, 32–50.

Kaufman, Y. J. (1993), Aerosol optical thickness and atmospheric path radiance, *J. Geophys. Res.*, *98*, 2677–2692, doi:10.1029/92JD02427.

Kim, D. H., B. J. Sohn, T. Nakajima, T. Takamura, T. Takemura, B. C. Choi, and S. C. Yoon (2004), Aerosol optical properties over east Asia determined from ground-based sky radiation measurements, *J. Geophys. Res.*, *109*, D02209, doi:10.1029/2003JD003387.

Knippertz, P., et al. (2009), Dust mobilization and transport in the northern Sahara during SAMUM 2006—A meteorological overview, *Tellus, Ser. B*, *61*, 12–31.

Kim, D., M. Chin, H. Yu, T. F. Eck, A. Sinyuk, A. Smirnov, and B. N. Holben (2011), Dust optical properties over North Africa and Arabian Peninsula derived from the AERONET dataset, *Atmos. Chem. Phys.*, *11*, 10,733–10,741, doi:10.5194/acp-11-10733-2011.

Koren, I., E. Ganor, and J. H. Joseph (2001), On the relation between size and shape of desert dust aerosol, *J. Geophys. Res.*, *106*, 18,047–18,054, doi:10.1029/2000JD900558.

Kubilay, N., T. Cokacar, and T. Oguz (2003), Optical properties of mineral dust outbreaks over the northeastern Mediterranean, *J. Geophys. Res.*, *108*(D21), 4666, doi:10.1029/2003JD003798.

Liu, Z., et al. (2008), CALIPSO lidar observations of the optical properties of Saharan dust: A case study of long-range transport, *J. Geophys. Res.*, *113*, D07207, doi:10.1029/2007JD008878.

Lyamani, H., F. J. Olmo, and L. Alados-Arboledas (2005), Saharan dust outbreak over southeastern Spain as detected by Sun photometer, *Atmos. Environ.*, *39*, 7276–7284.

Lyamani, H., F. J. Olmo, A. Alcántara, and L. Alados-Arboledas (2006), Atmospheric aerosols during the 2003 heat wave in southeastern Spain II: Microphysical columnar properties and radiative forcing, *Atmos. Environ.*, *40*, 6465–6476, doi:10.1016/j.atmosenv.2006.04.047.

Lyamani, H., F. J. Olmo, and L. Alados-Arboledas (2010), Physical and optical properties of aerosols over an urban location in Spain: Seasonal and diurnal variability, *Atmos. Chem. Phys.*, *10*, 239–254, doi:10.5194/acp-10-239-2010.

Mattis, I., V. Janenisch, D. Müller, K. Franke, and A. Ansmann (2000), Classification of particle extinction profiles derived within the framework of the German lidar network by the use of cluster analysis of back trajectories, in *Lidar Remote Sensing of the Atmosphere*, edited by A. Dabas, C. Loth, and J. Pelon, pp. 211–214, Ed. Ecole Polytech., Palaiseau, France.

Mishchenko, M. I., L. D. Travis, R. A. Kahn, and R. A. West (1997), Modeling phase functions for dustlike tropospheric aerosols using a shape mixture of randomly oriented polydisperse spheroids, *J. Geophys. Res.*, *102*, 16,831–16,847, doi:10.1029/96JD02110.

Mladenov, N., L. Alados-Arboledas, F. J. Olmo, H. Lyamani, A. Delgado, A. Molina, and I. Reche (2011), Applications of optical spectroscopy and stable isotope analyses to organic aerosol source discrimination in an urban area, *Atmos. Environ.*, *45*, 1960–1969, doi:10.1016/j.atmosenv.2011.01.029.

Müller, T., et al. (2009), Spectral absorption coefficients and imaginary parts of refractive indices of Saharan dust during SAMUM-1, *Tellus, Ser. B*, *61*, 78–95.

Muñoz, O., H. Volten, J. F. de Haan, W. Vassen, and J. W. Hovenier (2001), Experimental determination of scattering matrices of randomly oriented fly ash and clay particles at 442 and 633 nm, *J. Geophys. Res.*, *106*, 22,833–22,844, doi:10.1029/2000JD000164.

Nakajima, T., G. Tonna, R. Z. Rao, P. Boi, Y. Kaufman, and B. Holben (1996), Use of sky brightness measurements from ground for remote sensing of particulate polydispersions, *Appl. Opt.*, *35*, 2672–2686, doi:10.1364/AO.35.002672.

Olmo, F. J., A. Quirantes, A. Alcantara, H. Lyamani, and L. Alados-Arboledas (2006), Preliminary results of a non-spherical aerosol method for the retrieval of the atmospheric aerosol optical properties, *J. Quant. Spectrosc. Radiat. Transfer*, *100*, 305–314, doi:10.1016/j.jqsrt.2005.11.047.

Olmo, F. J., A. Quirantes, V. Lara, H. Lyamani, and L. Alados-Arboledas (2008), Aerosol optical properties assessed by an inversion method using the solar principal plane for non-spherical particles, *J. Quant. Spectrosc. Radiat. Transfer*, *109*, 1504–1516, doi:10.1016/j.jqsrt.2007.12.019.

Pace, G., A. di Sarra, D. Meloni, S. Piacentino, and P. Chamard (2006), Aerosol optical properties at Lampedusa (Central Mediterranean): 1.

Influence of transport and identification of different aerosol types, *Atmos. Chem. Phys.*, *6*, 697–713, doi:10.5194/acp-6-697-2006.
Papayannis, A., et al. (2008), Systematic lidar observations of Saharan dust over Europe in the frame of EARLINET (2000–2002), *J. Geophys. Res.*, *113*, D10204, doi:10.1029/2007JD009028.
Pereira, S. N., F. Wagner, and A. M. Silva (2011), Seven years of measurements of aerosol scattering properties, near the surface, in the southwestern Iberia Peninsula, *Atmos. Chem. Phys.*, *11*, 17–29, doi:10.5194/acp-11-17-2011.
Perrone, M. R., and A. Bergamo (2011), Direct radiative forcing during Sahara dust intrusions at a site in the Central Mediterranean: Anthropogenic particle contribution, *Atmos. Res.*, *101*, 783–798, doi:10.1016/j.atmosres.2011.05.011.
Petzold, A., et al. (2009), Saharan dust absorption and refractive index from aircraft-based observations during SAMUM 2006, *Tellus, Ser. B*, *61*, 118–130.
Pinker, R. T., H. Liu, S. R. Osborne, and C. Akoshile (2010), Radiative effects of aerosols in sub-Sahel Africa: Dust and biomass burning, *J. Geophys. Res.*, *115*, D15205, doi:10.1029/2009JD013335.
Prats, N., V. E. Cachorro, M. Sorribas, S. Mogo, A. Berjon, C. Toledano, A. M. De Frutos, J. de la Rosa, N. Laulainen, and B. A. de la Morena (2008), Columnar aerosol optical properties during "El Arenosillo 2004 summer campaign," *Atmos. Environ.*, *42*, 2643–2653, doi:10.1016/j.atmosenv.2007.07.041.
Prospero, J. M., and T. N. Carlson (1972), Vertical and aereal distribution of Saharan dust over the Western Ecuatorial North Atlantic Ocean, *J. Geophys. Res.*, *77*(27), 5255–5265, doi:10.1029/JC077i027p05255.
Prospero, J. M., P. Ginoux, O. Torres, S. E. Nicholson, and T. E. Gill (2002), Environmental characterization of global sources of atmospheric soil dust identified with the Nimbus 7 Total Ozone Mapping Spectrometer (TOMS) absorbing aerosol product, *Rev. Geophys.*, *40*(1), 1002, doi:10.1029/2000RG000095.
Querol, X., et al. (2004), Levels of particulate matter in rural, urban and industrial sites in Spain, *Sci. Total Environ.*, *334–335*, 359–376, doi:10.1016/j.scitotenv.2004.04.036.
Reagan, J. A., L. W. Thomason, B. M. Herman, and J. M. Palmer (1986), Assessment of atmospheric limitations on the determination of the solar spectral constant from ground-based spectroradiometer measurements, *IEEE Trans. Geosci. Remote Sens.*, *GE-24*, 258–266, doi:10.1109/TGRS.1986.289645.
Rodriguez, S., X. Querol, A. Alastuey, G. Kallos, and O. Kakaliagou (2001), Saharan dust contributions to PM10 and TSP levels in Southern and Eastern Spain, *Atmos. Environ.*, *35*, 2433–2447, doi:10.1016/S1352-2310(00)00496-9.
Rodriguez, S., A. Alastuey, S. Alonso-Perez, X. Querol, E. Cuevas, J. Abreu-Afonso, M. Viana, M. Pandolfi, and J. de la Rosa (2011), Transport of desert dust mixed with North African industrial pollutants in the subtropical Saharan Air Layer, *Atmos. Chem. Phys. Discuss.*, *11*, 8841–8892, doi:10.5194/acpd-11-8841-2011.
Rozwadowska, A., T. Zielinski, T. Petelski, and P. Sobolewski (2010), Cluster analysis of the impact of air back-trajectories on aerosol optical properties at Hornsund, Spitsbergen, *Atmos. Chem. Phys.*, *10*, 877–893, doi:10.5194/acp-10-877-2010.
Schladitz, A., T. Müller, N. Kaaden, A. Massling, K. Kandler, M. Ebert, S. Weinbruch, C. Deutscher, and A. Wiedensohler (2009), In situ measurements of optical properties at Tinfou (Morocco) during the Saharan Mineral Dust Experiment SAMUM 2006, *Tellus, Ser. B*, *61*, 64–78.
Silva, A. M., M. L. Bugalho, M. J. Costa, W. Von Hoyningen-Huene, T. Schmidt, J. Heintzenberg, and S. Henning (2002), Aerosol optical properties from columnar data during the second Aerosol Characterization Experiment on the south coast of Portugal, *J. Geophys. Res.*, *107* (D22), 4642, doi:10.1029/2002JD002196.
Sinyuk, A., et al. (2007), Simultaneous retrieval of aerosol and surface properties from a combination of AERONET and satellite data, *Remote Sens. Environ.*, *107*, 90–108, doi:10.1016/j.rse.2006.07.022.
Sokolik, I. N., and O. B. Toon (1999), Incorporation of mineralogical composition into models of the radiative properties of mineral aerosol from UV to IR wavelengths, *J. Geophys. Res.*, *104*, 9423–9444, doi:10.1029/1998JD200048.
Su, L., and O. B. Toon (2011), Saharan and Asian dust: Similarities and differences determined by CALIPSO, AERONET, and a coupled climate-aerosol microphysical model, *Atmos. Chem. Phys.*, *11*, 3263–3280, doi:10.5194/acp-11-3263-2011.
Sunnu, A., G. Afeti, and F. Resch (2008), A long-term experimental study of the Saharan dust presence in West Africa, *Atmos. Res.*, *87*, 13–26, doi:10.1016/j.atmosres.2007.07.004.
Tafuro, A. M., F. Barnaba, F. De Tomasi, M. R. Perrone, and G. P. Gobbi (2006), Saharan dust particle properties over the central Mediterranean, *Atmos. Res.*, *81*, 67–93, doi:10.1016/j.atmosres.2005.11.008.
Tegen, I., P. Hollrig, M. Chin, I. Fung, D. Jacob, and J. Penner (1997), Contribution of different aerosol species to the global aerosol extinction optical thickness: Estimates from model results, *J. Geophys. Res.*, *102*, 23,895–23,915, doi:10.1029/97JD01864.
Tesche, M., et al. (2009), Vertical profiling of Saharan dust with Raman lidars and airborne HSRL in southern Morocco during SAMUM, *Tellus, Ser. B*, *61*, 144–164.
Toledano, C., V. E. Cachorro, A. Berjon, A. M. de Frutos, M. Sorribas, B. A. de la Morena, and P. Goloub (2007a), Aerosol optical depth and Angstrom exponent climatology at El Arenosillo AERONET site (Huelva, Spain), *J. Quant. Spectrosc. Radiat. Transfer*, *133*, 795–807.
Toledano, C., V. E. Cachorro, A. M. de Frutos, M. Sorribas, N. Prats, and B. A. de la Morena (2007b), Inventory of African desert dust events over the southwestern Iberian Peninsula in 2000–2005 with an AERONET Cimel Sun photometer, *J. Geophys. Res.*, *112*, D21201, doi:10.1029/2006JD008307.
Toledano, C., V. E. Cachorro, A. M. de Frutos, B. Torres, A. Berjon, M. Sorribas, and R. S. Stone (2009), Airmass classification and analysis of aerosol types at El Arenosillo (Spain), *J. Appl. Meteorol. Climatol.*, *48*, 962–981, doi:10.1175/2008JAMC2006.1.
Toledano, C., et al. (2011), Optical properties of aerosol mixtures derived from sun-sky radiometry during SAMUM-2, *Tellus*, *63B*, 635–648.
Valenzuela, A., F. J. Olmo, H. Lyamani, A. Quirantes, and L. Alados-Arboledas (2011), Aerosol radiative properties retrieved during Saharan dust events in Southeastern Spain from 2005 to 2008, *Optica Pura y Aplicada*, *44*(4), 661–664.
Valenzuela, A., F. J. Olmo, H. Lyamani, M. Antón, A. Quirantes, and L. Alados-Arboledas (2012), Analysis of the desert dust radiative properties over Granada using principal plane sky radiances and spheroids retrieval procedure, *Atmos. Res.*, *104–105*, 292–301, doi:10.1016/j.atmosres.2011.11.005.
von Hoyningen-Huene, W., and P. Posse (1997), Nonsphericity of aerosol particles and their contribution to radiative forcing, *J. Quant. Spectrosc. Radiat. Transfer*, *57*(5), 651–668, doi:10.1016/S0022-4073(96)00153-7.
von Hoyningen-Huene, W., K. Wenzel, and S. Schienbein (1999), Radiative properties of desert dust and its effect on radiative balance, *J. Aerosol Sci.*, *30*, 489–502, doi:10.1016/S0021-8502(98)00074-3.
Wagner, F., et al. (2009), Properties of dust aerosol particles transported to Portugal from the Sahara desert, *Tellus, Ser. B*, *61*, 297–306.

L. Alados-Arboledas, M. Antón, H. Lyamani, F. J. Olmo, A. Quirantes, and A. Valenzuela, Departamento de Física Aplicada, Universidad de Granada, Fuentenueva s/n, E-18071 Granada, Spain. (avalenzuela@ugr.es)